LETTERS

Unique features of action potential initiation in cortical neurons

Björn Naundorf[1,2,3], Fred Wolf[1,2,3] & Maxim Volgushev[4,5]

Neurons process and encode information by generating sequences of action potentials[1,2]. For all spiking neurons, the encoding of single-neuron computations into sequences of spikes is biophysically determined by the cell's action-potential-generating mechanism. It has recently been discovered that apparently minor modifications of this mechanism can qualitatively change the nature of neuronal encoding[3,4]. Here we quantitatively analyse the dynamics of action potential initiation in cortical neurons *in vivo*, *in vitro* and in computational models. Unexpectedly, key features of the initiation dynamics of cortical neuron action potentials—their rapid initiation and variable onset potential—are outside the range of behaviours described by the classical Hodgkin–Huxley theory. We propose a new model based on the cooperative activation of sodium channels that reproduces the observed dynamics of action potential initiation. This new model predicts that Hodgkin–Huxley-type dynamics of action potential initiation can be induced by artificially decreasing the effective density of sodium channels. *In vitro* experiments confirm this prediction, supporting the hypothesis that cooperative sodium channel activation underlies the dynamics of action potential initiation in cortical neurons.

We analysed action potentials elicited in cortical neurons *in vivo* and *in vitro*, either spontaneously or in response to various stimuli. In all cells examined and for all conditions tested, the dynamics of action potential initiation was characterized by a very abrupt onset and a steep upstroke in membrane potential. In membrane potential traces, the abrupt onset of action potentials is apparent as a sharp kink (Fig. 1a, c). This phenomenon stands out even more clearly in phase plots that graph the rate of change of the membrane potential dV/dt against the instantaneous membrane potential $V(t)$, and is manifested as an almost vertical take-off in dV/dt versus V trajectories at action potential onset (Fig. 1b, d). In phase plots, an action potential is represented by a loop. At the start of the loop, the velocity increases rapidly from less than 5 mV ms^{-1} to more than 20 mV ms^{-1}. This several-fold increase in velocity occurs within a range of less than 1 mV and takes less than 0.2 ms. This onset behaviour is not a peculiarity of neurons *in vivo*. Neurons *in vitro* show similarly fast dynamics of action potential initiation (Fig. 1c, d). These dynamic features of recorded action potential onsets distinguish them from the behaviour of previously proposed computational models. Figure 1e, f shows a simulated action potential using a recently developed conductance-based model of a cortical neuron[5]. In this model, a velocity of 20 mV ms^{-1} is only reached over a range of 7–8 mV after about 1 ms. Thus, the real onset of cortical action potentials is approximately ten times faster than predicted by the model.

The rapid onset of action potentials is a very robust phenomenon, apparent during spontaneous and evoked activity *in vivo*. Moreover, it is independent of the temporal structure of synaptic inputs (Fig. 2) and of the electrophysiological cell class (Fig. 4). Fig. 2 shows phase plots and membrane potential traces from a simple cell (Fig. 2a, b) and a complex cell (Fig. 2c, d) recorded *in vivo* in cat visual cortex. In the phase plots, subthreshold membrane potential fluctuations are represented by a grey cloud. In both the simple and the complex cell, action potentials rise almost vertically out of this cloud. Detecting the point at which the rate of change reaches a value of 10 mV ms^{-1} thus allows reliable identification of the time of action potential initiation

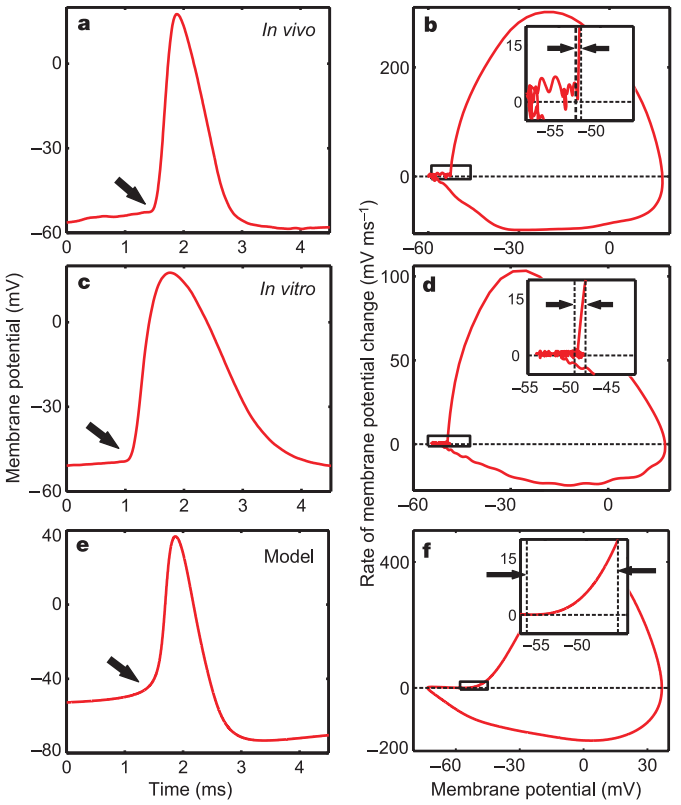

Figure 1 | Dynamics of action potential initiation in neocortical neurons and in a Hodgkin–Huxley-type model of a neocortical neuron. a, Action potential in a cat visual cortex neuron *in vivo*. The arrow shows the characteristic kink at action potential onset. **b**, Phase plot (dV/dt versus V) of the action potential from **a**. Inset shows the initial phase of the action potential. **c**, **d**, Action potential from a cat visual cortical slice *in vitro* at 20 °C. **e**, **f**, Action potential from a Hodgkin–Huxley-type model of a neocortical neuron[5].

[1]Max Planck Institute for Dynamics and Self-Organization, [2]Department of Physics and [3]Bernstein Center for Computational Neuroscience, University of Göttingen, Bunsenstr. 10, D-37073 Göttingen, Germany. [4]Department of Neurophysiology, Ruhr-University Bochum, D-44780 Bochum, Germany. [5]Institute of Higher Nervous Activity and Neurophysiology Russian Academy of Sciences, Moscow 117485, Russia.

and the onset potential. The phase plots also show a second salient feature of cortical action potentials: the onset potentials vary considerably, over ranges of up to 10 mV (Fig. 2a–d) (Special care was taken to exclude any non-stationarities, see Supplementary Information). This distinct variability in onset potentials has previously been observed in cat visual cortex[6–8] and rat hippocampus[9]. This second feature of cortical action potentials is also missing in Hodgkin–Huxley-type models. Figure 2e, f depicts the behaviour of such a model driven by fluctuating synaptic inputs[5]. The variability in onset potentials in this model is restricted to a range of less than 2 mV, which is much smaller than observed *in vivo*.

Two features thus render cortical action potentials distinctly different from simulated action potentials using Hodgkin–Huxley-type models. First, the initial action potential phase is approximately ten times faster in recorded neurons compared to conductance-based models. Second, the onset potential variability is approximately five times larger in the recorded cells. We tried, using various modifications of the models, to achieve a better match between recorded and simulated action potentials (including and/or modifying adaptation currents[10], channel stochasticity[11], state-dependent inactivation[12], sodium channel activation curves and peak conductances; see Supplementary Information). None of the modified models reproduced the two salient features of the recorded action potentials.

In fact, a straightforward analysis reveals that rapid action potential onset and large variability in onset potentials are strongly antagonistic in Hodgkin–Huxley-type models. In such models, the initial phase of an action potential is determined by the activation of voltage-dependent sodium channels. Their dynamics is described by the activation curve and kinetics of an associated gating variable. In the Hodgkin–Huxley formulation it can be shown that the rate of membrane depolarization is limited by $g_{Na}h_0m_\infty^3(V)(V_{Na}-V)/C + I_0/C$, where g_{Na} denotes peak sodium conductance, h_0 is the fraction of sodium channels available for activation, $m_\infty^3(V)$ is their activation curve, V_{Na} is the sodium reversal potential, C the membrane capacitance, and I_0 is the current carried by other channels. This upper bound on the rate of membrane potential change links the action potential onset dynamics directly to the width of the activation curve and peak sodium conductance. Figure 3 illustrates this relationship. An experimentally obtained activation curve from patches of cortical neurons[13,14] results in a shallow action potential onset (Fig. 3a, b). Increasing the steepness of the activation curve leads to sharper action potential onsets, but even with a fivefold increase, the simulated action potentials do not rise as fast as those recorded. Changing the effective peak sodium conductance—mimicking inactivation[6,9]—leaves the steepness of action potential onset unaffected but shifts the onset potentials (Fig. 3c, d). At the same time, increasing the steepness of the activation curve considerably decreases onset potential variability (Fig. 3c–f). Quantitatively, the variability of onset potentials is restricted by $\Delta V \approx k\log G$, where k is the width of the activation curve and G is the ratio of maximum to minimum peak conductance (see Supplementary Information). To mimic the measured combinations of onset rapidness and variability, unphysiologically large values of G (about 20,000) would be required.

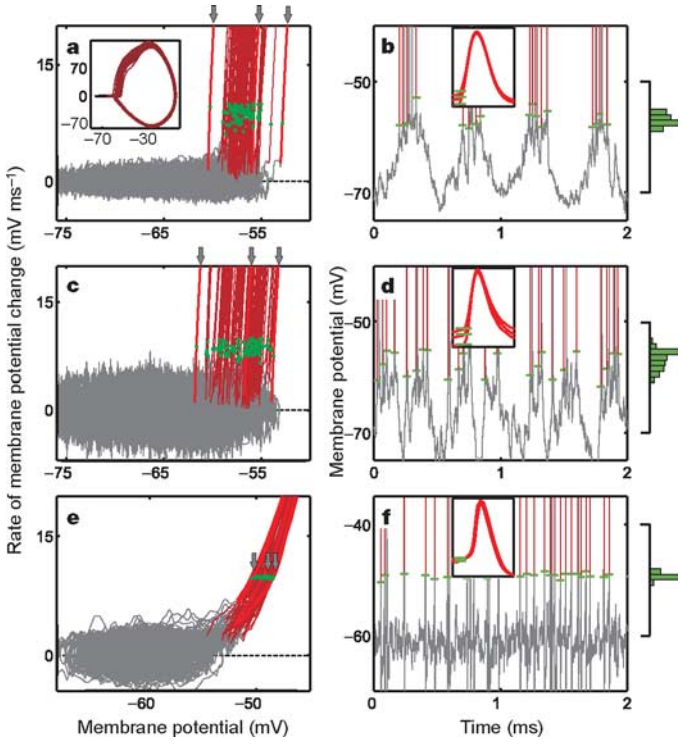

Figure 2 | Different action potential initiation in visual cortex neurons recorded *in vivo* and in a Hodgkin–Huxley-type model subject to fluctuating synaptic inputs. **a**, Phase plot of a simple cell response to a moving grating of optimal orientation. Subthreshold fluctuations are shown in grey, action potentials in red, and green dots indicate action potential onsets. The inset shows the complete trace. Arrows indicate three sample action potentials. **b**, Part of the recording from **a**, using the same colour code, with action potentials truncated in amplitude. Green bars show action potential onset potentials. Inset shows the action potentials marked with arrows in **a**. The histogram to the right shows the distribution of action potential onset potentials. **c**, **d**, Response of a complex cell. **e**, **f**, Response of a Hodgkin–Huxley-type model[5] subject to fluctuating synaptic input.

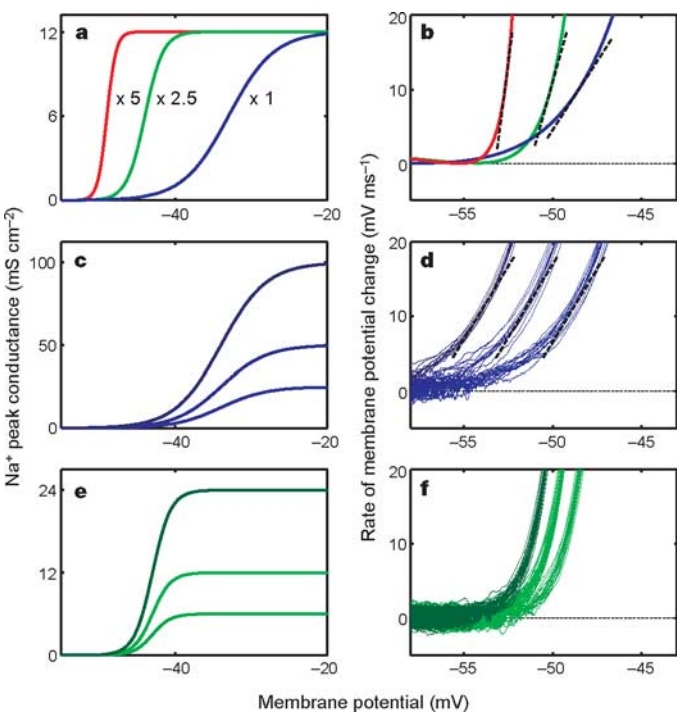

Figure 3 | Effect of the shape of the sodium channel activation curve and effective peak conductance on action potential initiation in a Hodgkin–Huxley-type model. Activation curves used in the model (**a**, **c**, **e**) and initial phases of resulting action potentials (**b**, **d**, **f**) are shown using matched colours. Blue lines show standard activation curves[14]. **a**, **b**, Increasing the steepness of the activation curve (**a**) leads to a more rapid action potential upstroke (**b**). Dashed lines indicate tangents at 10 mV ms^{-1}. **c**–**f**, Initiation of action potentials with shallow (**c**, **d**) and steep (**e**, **f**) activation curves and different sodium peak conductances in a model driven by fluctuating synaptic inputs (several action potentials superimposed). Changing peak conductance shifts the action potential onset potential but does not affect its onset rapidness. Steeper activation curves lead to smaller action potential onset spans (**d**, 6 mV; **f**, 2.5 mV).

To quantitatively compare the action potential onset dynamics in our recordings with action potential dynamics in Hodgkin–Huxley-type models, we plotted the action potential onset span (difference between maximum and minimum onset potential in a recording) against the rapidness of action potential onset (the slope of the phase plot at $dV/dt = 10\,mV\,ms^{-1}$) for real and simulated recordings (Fig. 4). In the simulations, we used two different models[5,10] driven by fluctuating synaptic currents. In both models we systematically changed the peak sodium conductance and the activation curve over the entire range in which action potentials were generated. The locations of data points from the model simulations reflect the antagonism between onset span and rapidness. Simulated action potentials either showed a large onset rapidness or a large onset span, but never both. The points representing simulated action potentials are clearly separated from the points representing *in vivo* action potentials, which show rapid onset dynamics and large variability in onset potentials, irrespective of the electrophysiological cell type. Action potentials recorded *in vitro* had similarly fast onset dynamics (Fig. 4).

The above arguments and our extensive simulations indicate that the dynamics of action potential initiation in cortical neurons deviates qualitatively from the classical picture described by the Hodgkin–Huxley framework. What could be the biophysical mechanism that enables cortical action potentials to initiate much faster and at the same time with a much larger onset potential variability than predicted by the Hodgkin–Huxley theory? According to this theory, there is a one-to-one relationship between the single-channel activation curve and the action potential onset dynamics, owing to the assumption that the opening of individual sodium channels is statistically independent. This assumption, however, might be violated in the highly organized molecular machinery of a living cell. Indeed, the rapid onset of action potentials suggests that many sodium channels open virtually simultaneously, that is, in a potentially cooperative fashion.

To assess whether cooperative activation of voltage-gated sodium channels can account for the two characteristic features of cortical action potential initiation, we constructed a model of a population of coupled sodium channels. In this model, the gating of individual sodium channels follows a scheme introduced by Aldrich, Corey, and Stevens[15]. It incorporates state-dependent inactivation from the open state and voltage-dependent inactivation from closed states[15,16]. The key feature of our model is a coupling between neighbouring channels: the opening of a channel shifts the activation curve of each channel to which it is coupled towards more hyperpolarized values, thus increasing its probability of opening.

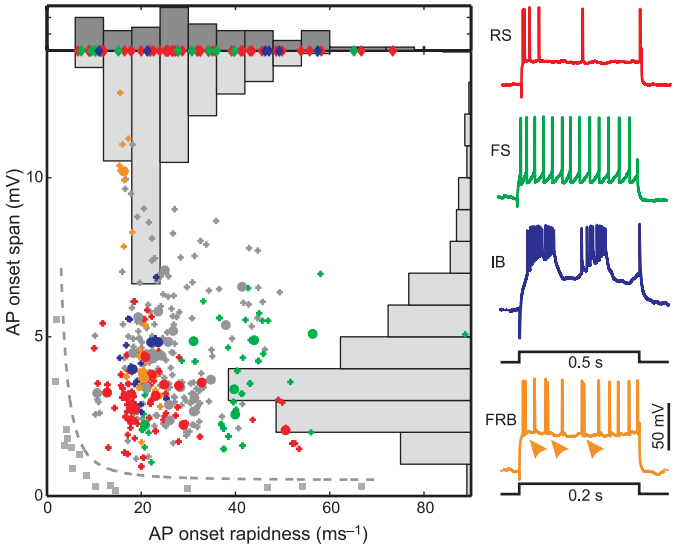

Figure 4 | Action potential onset span and rapidness in cortical neurons and Hodgkin–Huxley-type models. Points show data from cat visual cortex neurons *in vivo*, classified electrophysiologically as regular spiking (RS), fast spiking (FS), intrinsically bursting (IB) or fast rhythmic bursting (FRB). Colours match the neuronal responses to current steps shown on the right. Grey points indicate electrophysiologically unidentified cells. Circles show the mean of several measurements for each cell (individual measurements indicated with crosses). Diamonds at the top of the panel show *in vitro* data (cat visual cortex in blue, rat visual cortex in red, mouse hippocampus in green). Grey squares show simulation results from two Hodgkin–Huxley-type models with varied sodium channel activation curves and peak conductances, driven by fluctuating synaptic inputs. Dashed grey line separates the model from experimentally derived data. Histograms show the marginal distributions of the *in vivo* (light grey bars) and *in vitro* (dark grey bars) data.

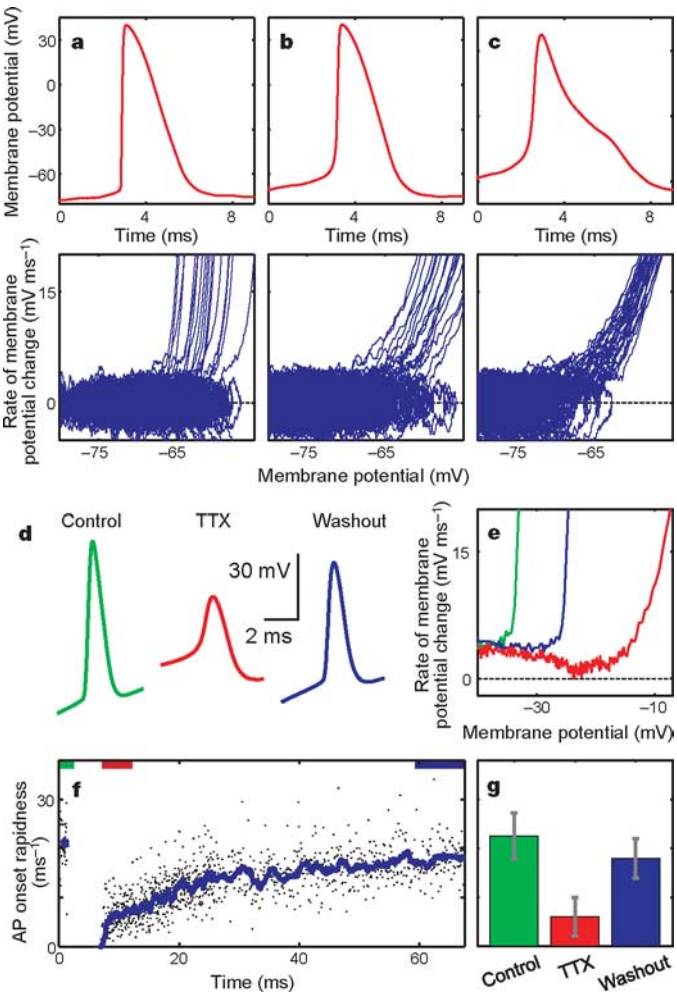

Figure 5 | Cooperative activation of voltage-gated sodium channels can account for the dynamics of action potential initiation in cortical neurons. **a**, Waveform (top) and phase plot (bottom) of action potentials elicited by fluctuating inputs in a conductance-based model that incorporates cooperative activation of sodium channels and closed-state inactivation. Both the action potential onset potential variability and onset rapidness are comparable to the *in vivo* recordings in Fig. 2. **b**, **c**, Same model, but without inter-channel coupling (**b**), and with Hodgkin–Huxley-like channel activation (**c**). **d**–**g**, Reducing the effective density of available sodium channels through TTX application reversibly reduces action potential amplitude and onset rapidness in cortical neurons *in vitro*. Shown are action potential waveforms (**d**) and phase plots of their initial parts (**e**). **f**, Time course of action potential onset rapidness in a cortical neuron before, during and after TTX application. **g**, Reversible reduction in onset rapidness of action potentials by TTX in six neurons. Error bars indicate s.e.m.

This model is able to reproduce the key features of cortical action potential initiation (Fig. 5a–c). With strongly cooperative activation, voltage-dependent inactivation from closed states, and slow de-inactivation (recovery from inactivation) of sodium channels, the simulated action potentials show both a large onset rapidness and large variability in onset potentials (Fig. 5a). Turning off the inter-channel coupling made the onset dynamics much shallower, while leaving onset variability unaffected (Fig. 5b). Hodgkin–Huxley-type dynamics of action potential onset was recovered when inactivation and de-inactivation were set to be fast and voltage-independent (Fig. 5c).

Assuming that channel interactions are distance-dependent in neuronal membranes, our model predicts that reducing the effective density of channels should weaken cooperativity, reduce the action potential onset rapidness and eventually lead to Hodgkin–Huxley-type onset dynamics. We tested this prediction *in vitro*, recording action potentials while reducing the density of available sodium channels by the application of tetrodotoxin (TTX). As expected, TTX application led to a decrease in action potential amplitude (Fig. 5d). More importantly, it also led to a substantial reduction in the onset rapidness of action potentials (Fig. 5d, e) in all tested cortical neurons (Fig. 5g), as predicted by our model. Moreover, gradual recovery of the number of available sodium channels during washout of TTX led to a gradual increase in action potential onset rapidness (Fig. 5f). These results cannot be explained by Hodgkin–Huxley-type models, in which reduction in the sodium channel density modifies only the amplitude of action potentials and their onset potential, but not their onset rapidness (see Fig. 3). Thus, in our opinion the fact that the dynamics of action potential initiation deviates qualitatively from voltage-dependent single channel activation points towards the cooperative activation of voltage-gated sodium channels.

Although our results are unexpected from a biophysical perspective, the combination of rapid dynamics and variable onset potentials of action potentials is beneficial for the coding of fast signals[3,4] (see also Supplementary Information). With Hodgkin–Huxley-type dynamics of action potential initiation, the encoding of signals that vary on a timescale of less than 10 ms requires unphysiologically high mean firing rates that are likely to be energetically prohibitive[17,18]. With action potential onset dynamics as described here for cortical neurons, much lower mean firing rates can support the encoding of such rapidly varying signals.

METHODS

***In vivo* and *in vitro* experiments.** *In vivo* intracellular recordings were made using sharp electrodes in adult cats (3.0–4.5 kg). Data from 47 cells were used for the analysis. In each cell, we recorded responses to the presentation of moving gratings of different orientations (duration 5–7 s), and periods of spontaneous activity (10–120 s). Cells were classified functionally as either simple or complex using the spike response modulation index, and electrophysiologically by their responses to depolarizing current steps. *In vitro*, whole-cell recordings were made with patch electrodes in slices of rat or cat visual cortex and rat or mouse hippocampus. Data from 17 rat, 3 mouse and 2 cat neurons were analysed.

Computational models. We used two conductance-based Hodgkin–Huxley-type models[5,10], constructed to match the subthreshold membrane potential dynamics and firing statistics of cortical neurons. We introduced modifications to the models and varied model parameters over wide ranges in an attempt to reproduce the experimentally observed dynamics of action potential initiation. Action potential initiation by cooperative sodium channel activation was modelled using an effective mean field dynamics for a population of interacting sodium channels.

Details of experimental procedures and data analysis, and definitions of the models, their modifications and parameter ranges are provided in the Supplementary Information.

Received 22 October 2005; accepted 27 January 2006.

1. Bernstein, J. Ueber den zeitlichen Verlauf der negativen Schwankung des Nervenstroms. *Pflugers Arch.* **1,** 173–207 (1868).
2. Huxley, A. F. *Nobel Lectures, Physiology or Medicine 1963–1970* (Elsevier, Amsterdam, 1972).
3. Fourcaud-Trocmé, N., Hansel, D., van Vreeswijk, C. & Brunel, N. How spike generation mechanisms determine the neuronal response to fluctuating inputs. *J. Neurosci.* **23,** 11628–11640 (2003).
4. Naundorf, B., Geisel, T. & Wolf, F. Action potential onset dynamics and the response speed of neuronal populations. *J. Comput. Neurosci.* **18,** 297–309 (2005).
5. Destexhe, A. & Paré, D. Impact of network activity on the integrative properties of neocortical pyramidal neurons *in vivo*. *J. Neurophysiol.* **81,** 1531–1547 (1999).
6. Azouz, R. & Gray, C. M. Dynamic spike threshold reveals a mechanism for synaptic coincidence detection in cortical neurons *in vivo*. *Proc. Natl Acad. Sci. USA* **97,** 8110–8115 (2000).
7. Volgushev, M., Pernberg, J. & Eysel, U. T. A novel mechanism of response selectivity of neurons in cat visual cortex. *J. Physiol. (Lond.)* **540,** 307–320 (2002).
8. Azouz, R. & Gray, C. M. Adaptive coincidence detection and dynamic gain control in visual cortical neurons *in vivo*. *Neuron* **37,** 513–532 (2003).
9. Henze, D. A. & Buzsaki, G. Action potential threshold of hippocampal pyramidal cells *in vivo* is increased by recent spiking activity. *Neuroscience* **105,** 121–130 (2001).
10. Wang, X. J., Liu, Y., Sanchez-Vives, M. V. & McCormick, D. A. Adaptation and temporal decorrelation by single neurons in the primary visual cortex. *J. Neurophysiol.* **89,** 3279–3293 (2003).
11. Schneidman, E., Freedman, B. & Segev, I. Ion channel stochasticity may be critical in determining the reliability and precision of spike timing. *Neural Comput.* **10,** 1679–1703 (1998).
12. Patlak, J. Molecular kinetics of voltage-dependent Na^+ channels. *Physiol. Rev.* **71,** 1047–1080 (1991).
13. Huguenard, J. R., Hamill, O. P. & Prince, D. A. Developmental changes in Na^+ conductances in rat neocortical neurons: appearance of a slowly inactivating component. *J. Neurophysiol.* **59,** 778–795 (1988).
14. Colbert, C. M. & Pan, E. Ion channel properties underlying axonal action potential initiation in pyramidal neurons. *Nature Neurosci.* **5,** 533–538 (2002).
15. Aldrich, R. W., Corey, D. P. & Stevens, C. F. A reinterpretation of mammalian sodium channel gating based on single channel recording. *Nature* **306,** 436–441 (1983).
16. Goldman, L. Stationarity of sodium channel gating kinetics in excised patches from neurobastoma N1E 115. *Biophys. J.* **69,** 2364–2368 (1995).
17. Attwell, D. & Laughlin, S. B. An energy budget for signaling in the grey matter of the brain. *J. Cereb. Blood Flow Metab.* **21,** 1133–1145 (2001).
18. Lennie, P. The cost of cortical computation. *Curr. Biol.* **13,** 493–497 (2003).

Supplementary Information is linked to the online version of the paper at www.nature.com/nature.

Acknowledgements We would like to thank A. Borst, M. Brecht, M. Chistiakova, T. Geisel, T. Kottos, T. Moser, E. Neher, W. Stühmer, I. Timofeev and C. van Vreeswijk for discussions, A. Borst, M. Brecht and E. Neher for comments on earlier versions of the manuscript, and A. Malyshev for help in some of the experiments. This study was supported by grants from the Deutsche Forschungsgemeinschaft to M.V., by grants from the Human Frontier Science Program and the Bundesministerium für Bildung und Forschung to F.W., and by the Max-Planck Society.

Author Contributions B.N., F.W. and M.V. contributed equally to this work. All authors discussed the results and commented on the manuscript.

Author Information Reprints and permissions information is available at npg.nature.com/reprintsandpermissions. The authors declare no competing financial interests. Correspondence and requests for materials should be addressed to F.W. (fred@chaos.gwdg.de).

Unique features of action potential initiation in cortical neurons

Björn Naundorf, Fred Wolf, Maxim Volgushev

Online supplementary information (Part 1 of 3):

Experimental methods and data analysis

In this part of the Supplementary Information we describe in detail all experimental and data analysis methods used in this study. This includes a description of the stationarity criteria for MP recordings and the estimation of AP (action potential) onset potentials and rapidness. We characterize our data sample, and show that rapid AP onset and substantial variability of AP onset potential are found in all cortical cell classes and argue that they are genuine characteristics of cortical neurons.

Contents

Experimental methods 2

Data sample 5

Data analysis 7

Action potential onset rapidness and onset variability are genuine properties of cortical neurons 9

References 12

Experimental methods

All experimental procedures used in this study were in accordance with the guidelines published in the European Communities Council Directive (86/609/EEC, 1986) and were approved by a local animal welfare committee (Bezirksregierung Arnsberg, Germany).

In vivo intracellular recordings were made in adult cats (3.0-4.5 kg). Surgery and animal maintenance were similar to those used in our previous studies (Volgushev et al., 2000, 2002). Anaesthesia was induced with a mixture of ketamine hydrochloride (Ketanest, Parke-Davis GmbH, Germany, 0.3 ml/kg, i.m.) and Rompun (Bayer, Germany, 0.08 ml/kg, i.m.). Surgery was started after stable anaesthesia with complete analgesia was achieved. Sometimes this required additional doses of the anaesthetic. After tracheal and arterial cannulations, the animal was placed in a stereotaxic frame, the skull was exposed and a craniotomy (about 5 mm diameter) was done over area 17 of the visual cortex centred at P4/L3 (Horsley-Clark). A brass-cylinder (diameter 20 mm) was cemented over the opening. The hydraulically driven microelectrode holder (Narishige Instruments, Japan) was mounted directly onto the skull with screws and dental cement. All wound edges and pressure points were treated with a local anaesthetic (Xylocaine, Astra GmbH, Germany) every 5-8 hours. Muscle relaxation with alcuronium chloride (Alloferin, ICN Pharmaceuticals, Germany) and artificial respiration were started either at this point, or earlier during the surgery, to avoid respiratory depression due to additional doses of the anaesthetic. Thereafter adequate anaesthesia was maintained throughout the experiment by a gas mixture of N_2O:O_2 (70:30) and 0.2-0.4% halothane (Eurim-Pharm, Germany). Artificial respiration was performed with a cat/rabbit ventilator

(Model 6025, Ugo Basile, Biological Research Apparatus, Comaria-Varese Italy). The volume (20-40 cm^3) and the rate of stroke (7-15 per minute) were adjusted to maintain end-tidal CO_2 between 3.5 and 4.0%. End-tidal CO_2, body temperature, heart rate, blood pressure and EEG were continuously monitored. Body temperature was maintained around 37-38°C. Fluid replacement was achieved by the intraarterial administration of 6 ml of Ringer solution containing 1.25% glucose, per hour. Paralysis was maintained by i.a. infusion of alcuronium chloride (0.15 mg/kg/h) in Ringer's solution. The experiments lasted usually 2-4 days. At the end of the experiment, animals were sacrificed with an overdose of anaesthetics.

In vivo intracellular recordings from visual cortical neurons were made with sharp electrodes filled with 2.5M potassium acetate, or 1M potassium acetate and 1% biocytin (Sigma-Aldrich GmbH, Germany). Electrode resistance was 70-120 MΩ. After amplification (Axoclamp 2B, Axon Instruments, USA, and additional DC-amplifier, total gain x20 to x100) and low-pass filtering at 3-5 kHz, the data were digitized at 10-40 kHz and stored on a computer (PC-586; Spike-2, Cambridge Electronic Design, Great Britain). Visual stimuli (moving gratings of different orientation and direction of movement) were generated on the screen of a second computer using subroutines of the Vision Works stimulation system (Cambridge Research Systems, New Hamshire, USA). Parameters of visual stimulation, sequence of stimuli (randomized) and communication to the data acquisition computer were controlled by custom-written software. The screen was positioned 57 cm in front of the animal and was focussed on the retina using appropriate lenses. Background illumination was 2.37 cd/m^2. Luminance of the dark and light stimuli was 0.02 and 12.8 cd/m^2, respectively. Stimuli were presented monocularly to the dominant eye. Cells were classified as simple or complex according to standard criteria (Orban, 1984) and by using the spike response modulation index, defined as a half of the

peak-to-peak modulation divided by the mean increase of the spiking frequency during presentation of an optimal moving grating (Dean & Tolhurst, 1983; Skottun et al., 1991).

In vitro intracellular recordings were made in slices of rat or cat visual cortex and rat and mice hippocampus. The details of slice preparation and recording were similar to those previously used (Volgushev et al., 2000). The Wistar rats or mice (P21-P35 Charles River GmbH, Suzfeld, Germany) were anaesthetized with ether, decapitated and the brain was rapidly removed. One hemisphere was mounted onto an agar block and 350-400 μm thick sagittal slices containing the visual cortex and/or hippocampus were cut with a vibrotome (TSE, Kronberg, Germany or Leica, Bensheim, Germany) in ice cooled oxygenated solution. Slices of the cat visual cortex were prepared from brains obtained at the end of acute *in vivo* experiments in which one of the hemispheres remained intact. The animal was deeply anaesthetised by increasing halothane concentration in a N_2O:O_2 (70:30) gas mixture to 3-3.5% and perfused with an ice-cooled oxygenated solution of the same ionic composition as that used for slice preparation. The visual cortex of the intact hemisphere was exposed, and a block of tissue containing the visual cortex was cut, removed from the cat, and slices (400-500 μm) were prepared as above. After cutting, the slices were placed into an incubator where they recovered for at least one hour at room temperature before moving on of them in the recording chamber. The solution used during the preparation of the slices had the same ionic composition as the perfusion/ extracellular solution. It contained (in mM) 125 NaCl, 2.5 KCl, 2 $CaCl_2$, 1 $MgCl_2$, 1.25 NaH_2PO_4, 25 $NaHCO_3$, 25 D-glucose and bubbled with 95% O_2 and 5% CO_2. Recordings were made with the slices in submerged conditions at 32-35°C or at room temperature. Recordings at room temperature were performed to check if this factor

was critical for the observed fast dynamics of action potential initiation. Temperature in the recording chamber was monitored with a thermocouple positioned close to the slice, 2-3 mm from the recording site. In experiments with tetrodotoxin (TTX), it was added to the extracellular solution at concentrations 10-300 nM. Whole-cell recordings using patch electrodes were made from neurons of different morphology (pyramidal, non-pyramidal) and located in different layers, selected under visual control using Nomarski optics and infrared videomicroscopy (Dodt & Zieglgänsberger, 1990; Stuart, Dodt & Sakmann, 1993). The patch electrodes were filled with K-gluconate based solution (in mM: 127 K-Gluconate, 20 KCl, 2 $MgCl_2$, 2 Na_2ATP, 10 HEPES, 0.1 EGTA and 0.3-1.0% biocytin) and had a resistance of 3-6 MΩ. Action potentials were evoked by depolarising current steps or by synaptic stimulation. Synaptic responses were evoked by electric shocks applied through bipolar stimulation electrodes located 0.5-1.5 mm below or lateral to the recording site. After amplification using Axoclamp-2A (Axon Instruments), and low-pass filtering at 3-5 kHz, data were digitised at 10-40 kHz and fed into a computer (PC-486; Digidata 1200 interface and pCLAMP software, Axon Instruments). The EGTA, HEPES, potassium gluconate, Na_2ATP and TTX were obtained from Sigma, and the remaining chemicals were obtained from JT Baker BV (Deventer, Holland).

Data sample

The sample of neurons analysed contained different types of cells. In the *in vivo* data from cats, we classified some of the recorded cells electrophysiologically, according to their intrinsic membrane properties, which were assessed from responses to injection of depolarising current steps. All electrophysiological types of cells described so far in the neocortex were represented in our sample, including regular

spiking (RS), fast spiking (FS), intrinsically bursting (IB) and chattering or fast rhythmic bursting (FRB) neurons (Fig. 4 in the paper). Some of the neurons were labelled with biocytin during the recording. Among these neurons, cells of different morphological types and different location within cortical layers were encountered. Microphotographs in Fig. 1SI give examples of a layer V pyramidal cell, a layer IV spiny stellate cell and a layer III pyramidal cell from our sample.

In vitro recordings were made in slices of rat and cat neocortex and rat and mouse hippocampus. We made whole cell recordings with patch electrodes under visual control. This allowed visual pre-selection of cells of different morphological types and layer location. According to the classification based on the intrinsic membrane properties, three types of neocortical neurons were encountered *in vitro*: regular spiking (RS), fast spiking (FS) and intrinsically bursting (IB) cells.

The diversity of our *in vivo* and *in vitro* data, which include cortical neurons of different morphology, layer location and intrinsic membrane properties, makes the sample representative.

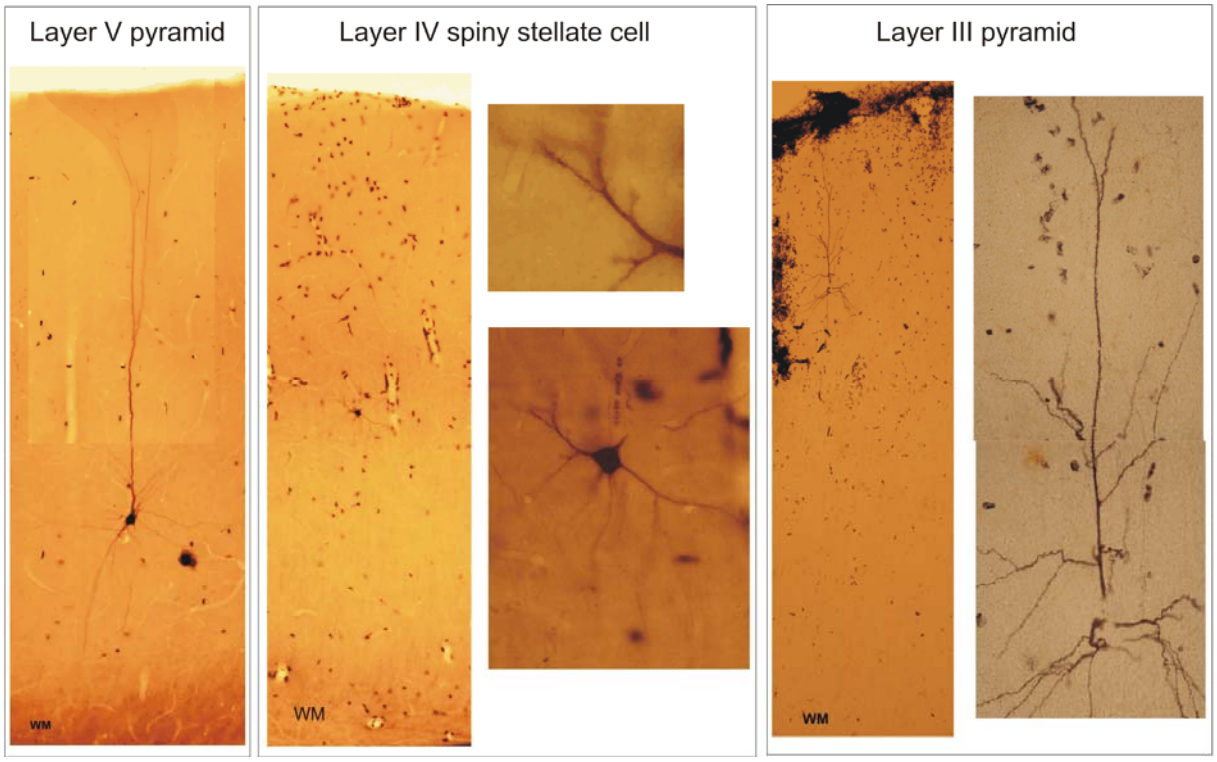

Fig 1SI: Microphotographs of examples of a Layer V pyramidal cell, a layer IV spiny stellate cell and a layer III pyramidal cell from our sample. In each panel, the images to the right were taken at larger magnifications.

Data analysis

We analyzed data from 47 cells recorded *in vivo*. In each cell, we recorded responses to the presentation of moving gratings of different orientations (duration 5-7s), and periods of spontaneous activity (10-120s). Altogether, we analyzed 409 *in vivo* recordings. For comparison, we also examined data from 22 cells recorded in slices (17 in rat, 3 in mouse, 2 in cat), resulting in 70 *in vitro* recordings.

Each recording contained at least 5 action potentials (APs), and the AP onset potentials and AP peak amplitudes fulfilled the following stationarity criterion. The stationarity of each recording was tested by computing the standard deviation of the values of the MP, the AP peak potentials and the onset potentials for increasing window sizes ranging from 100ms to 7s. A recording was classed as stationary if

the average standard deviation in peak amplitude and spike onset potential differed by less than 10% for window sizes between 100ms and 7s.

All of our recordings fulfilled this criterion and did not exhibit slow drifts of the MP, of the AP onset or peak potential.

All recordings were interpolated to a resolution of $\Delta t = 10\mu s$ using the Matlab pchip interpolation filter (Matlab V6.5 (R13)). For each interpolated recording, we computed the temporal derivative *dV/dt*:

(1) $$\frac{dV}{dt}(t_n) = (V_{n+1} - V_{n-1})/(2\Delta t)$$

In Fig 1-3, this temporal derivative is graphed against the instantaneous MP, yielding a "phase plot" representation (see main text).

In each recording, we first detected APs using a voltage threshold set at –30mV. For each AP, we then determined the onset potential using as a criterion the point where the velocity of the AP exceeded 10mV/ms. For all analyses, we took only APs into account that were separated from preceding APs by more than 30ms.

The AP onset rapidness shown in Fig. 4 was determined as follows: For each AP a line was fitted to the AP curve in the phase plane (*V vs. dV/dt)* representation at *dV/dt*=10 mV/ms. The slope of this line is defined as the onset rapidness of a single AP. The onset rapidness for a recording is then given as the mean onset rapidness of all APs in the recording. The onset rapidness *in vitro* was measured at temperatures 32-35°C and at room temperature. The AP onset span of a recording is defined as the difference between maximum and minimum AP onset potential. In *in vitro* experiments, APs were mostly elicited by constant current injections and the

membrane potential exhibited no fluctuations. Thus the onset span was assessed only *in vivo*.

Action potential onset rapidness and onset variability are genuine properties of cortical neurons

In the paper, we show that the large AP onset rapidness together with the large AP onset potential variability observed in *in vivo* intracellular recordings from cortical neurons is outside the range of behaviours that can be described by Hodgkin-Huxley type models. We are not the first to observe these features of cortical APs per se. Sharp, step-like onsets of action potentials recorded *in vivo* can be seen in previous publications from several laboratories, as soon as APs are shown at fine temporal resolution (see for example, cat visual cortex: Fig. 2 in Gray, McCormick 1996 Science 274:109-113; Fig. 5 D,E in Bringuier et al., J.Physiology 1997, 500:751-774; Fig. 2A in Azouz, Gray 1999; cat somatosensory cortex: Fig. 6D, 8B in Yamamoto et al 1990, Exp. Brain Res. 80:12-22; rat somatosensory cortex: Fig.11 in Brecht et al., J. Physiology 2003 553:243-265; cat area 7: Fig. 4 in Timofeev et al., Neuroscience 2002, 114:1115-1132). Also the large variability of AP onset potentials has been reported before (Azouz, Gray 1999, 2000; Volgushev et al. 2002) and can be seen in many of the examples cited above. Nevertheless, it is important to assure that these features represent genuine properties of cortical neurons and are not caused by experimental manipulations or other artefacts.

In is hard to imagine that the large AP onset rapidness represents a measurement artefact. First, the recording circuit in electrophysiological experiments exhibits properties of a low pass filter due to resistance and capacitance of the recording electrode. It is thus expected to rather wash out rapid acceleration of membrane

potential changes. Second, rapid AP onsets are observed using both sharp and patch electrodes, that differ considerably in their electrical properties. Third, direct evidence that rapid AP onsets are not induced by measurement apparatus comes from the *in vitro* experiments with TTX described in the paper (Fig.5). There, the AP onset dynamics was observed to change from *in vivo*-like rapid onsets in control conditions to gradual Hodgkin-Huxley type onsets during application of low concentrations of TTX and back to rapid onsets upon washout of the drug. These reversible modifications of AP onsets were observed in every cell tested with TTX, in an unmodified setup and under continuous recoding. Together these observations indicate that large AP onset rapidness is a genuine property of cortical neurons.

Various lines of evidence from our experiments as well as published results of other labs indicate that the variability of AP onset potentials is also not of an artefactual nature. In principle, it is conceivable that a non-stationary potential drop between the reference electrode and the extracellular space of the measured cell or a non-stationary state of the measurement electrode might bias the variance of AP onset potentials towards increased values. However, these factors would manifest themselves as systematic trends. Further, such general changes of electrode offset potential would shift all measured potential values, including mean membrane potential and AP peak. In our analyses, we therefore applied strict stationarity criteria such that all quantifications of AP onset dynamics were based on recordings that were very stable (c.f. above). Examples of widely different AP onset potentials obtained under stationary recording conditions are apparent in Figure 2 (inset). There three APs were superimposed such that the times of peak potentials were aligned. While the peak potentials of the APs are virtually identical, the onset potentials of the three APs differ by up to 8mV For our data, this is a representative example. In

general, we find that AP peak and onset potentials are often uncorrelated (data not shown). Additional evidence that AP onset variability is not due to recording non-stationarity, but is a genuine property of neocortical neurons is provided by the fact that onset potentials of two APs directly succeeding one another and separated by short inter-spike-intervals (<25 ms) are substantially different, as predicted by incomplete deinactivation of sodium channels. We note here, that to exclude the influence of this type of variability we did not include in our analyses the APs appearing less than 30 ms after the preceding spike. Furthermore, similar AP onset potential variability was recently observed *in vitro* in dynamic clamp experiments (de Polavieja et al., 2005) that were designed to minimize sources of non-stationarity. De Polavieja stimulated cortical neurons with temporally fluctuating inputs and observed onset potential variability indistinguishable from *in vivo* recordings. In such *in vitro* experiments the stability of the potential measurement is well controlled and AP onset potential variability is observed even if the stability of the recording is maximized by using double-electrode impalement of single neurons, where one electrode is used for membrane potential measurement and another one for dynamical electrical stimulation.

In summary, these facts show that rapid AP onsets and large variability of AP onset potentials are robust phenomena reproducible under a wide variety of recording conditions. Most importantly, AP onset rapidness can be artificially and reversibly turned down in cells recorded *in vitro*. Large AP onset potential variability is observed even if the stationarity of the recording is controlled to the highest possible degree. We are thus confident that large AP onset rapidness and onset potential variability are genuine features of AP initiation in cortical neurons.

References

Azouz, R., Gray, C.M. Adaptive coincidence detection and dynamic gain control in visual cortical neurons *in vivo*. *Neuron* 37, 513-532 (2003).

Brecht M, Roth A, Sakmann B. Dynamic receptive fields of reconstructed pyramidal cells in layers 3 and 2 of rat somatosensory barrel cortex. J. Physiol. 553, 243-65 (2003)

Bringuier V, Fregnac Y, Baranyi A, Debanne D, Shulz DE. Synaptic origin and stimulus dependency of neuronal oscillatory activity in the primary visual cortex of the cat. J. Physiol. 500, 751-74 (1997)

Dean, A.F. & Tolhurst, D.J. On the distinctness of simple and complex cells in the visual cortex of the cat. J. Physiol. 344, 305-325 (1983)

Dodt, H.U. & Zieglgänsberger W. Visualizing unstained neurons in living brain slices by infrared DIC-videomicroscopy. Brain Res. 537, 333-336 (1990).

Gray CM, McCormick DA. Chattering cells: superficial pyramidal neurons contributing to the generation of synchronous oscillations in the visual cortex. Science. 4 109-13 (1996)

de Polavieja GG, Harsch A, Kleppe I, Robinson HP, Juusola M. Stimulus history reliably shapes action potential waveforms of cortical neurons. J. Neurosci. 2005, 25, 5657-65 (2005)

Skottun, B.C. et al. Classifying simple and complex cells on the basis of response modulation. Vision Res. 31, 1079-1086 (1991)

Stuart, G.J., Dodt, H.U., Sakmann, B. Patch-clamp recordings from the soma and dendrites of neurons in brain slices using infrared video microscopy. Pflugers Arch. 423, 511-518 (1993).

Timofeev I, Grenier F, Steriade M. The role of chloride-dependent inhibition and the activity of fast-spiking neurons during cortical spike-wave electrographic seizures. Neurosci. 114, 1115-32 (2002).

Volgushev, M., Vidyasagar, T.R., Chistiakova, M., Yousef, T. & Eysel, U.T. Membrane properties and spike generation in rat visual cortical cells during reversible cooling. J. Physiol., 522, 59-76 (2000).

Volgushev, M., Pernberg, J. & Eysel, U.T. Comparison of the selectivity of postsynaptic potentials and spike responses in cat visual cortex. Europ. J. Neurosci. 12, 257-263 (2000).

Volgushev, M., Pernberg, J. & Eysel, U.T. A novel mechanism of response selectivity of neurons in cat visual cortex. J. Physiol. 540, 307-320 (2002).

Yamamoto T, Samejima A, Oka H. The mode of synaptic activation of pyramidal neurons in the cat primary somatosensory cortex: an intracellular HRP study. Exp. Brain Res. 80, 12-22 (1990).

Unique features of action potential initiation in cortical neurons

Björn Naundorf, Fred Wolf, Maxim Volgushev

Online supplementary information (Part 2 of 3):

Hodgkin-Huxley type models

In this part of the Supplementary Information we describe the Hodgkin-Huxley type conductance based models used in the study and the modifications which were applied to these models, such as changes of sodium channel activation curves and single channel stochasticity. We also describe parameter ranges explored. Finally, we show that rapidness and onset potential variability of AP initiation are strongly antagonistic in the whole class of Hodgkin-Huxley type conductance based models.

Contents

Hodgkin-Huxley type conductance based models 2

Model A (Destexhe et al.) 2

Robustness against variations in model parameters and structure 3

Model B: Adaptation currents and AP initiation (Wang et al.) 4

Channel noise and AP initiation 7

AP onset variability and steepness are antagonistic in Hodgkin-Huxley type models 12

Hodgkin-Huxley type conductance based models

For the simulations, we used two different models (Model A and B), which were constructed to match the subthreshold MP dynamics and the firing statistics of cortical neurons.

Model A (Destexhe et al.)

Model A is a single compartment Hodgkin-Huxley type neuron model (Destexhe et al, 1999). As shown by Destexhe et al.,1999, this model reproduces the statistics of MP fluctuations and spike-trains of neocortical neurons *in vivo*. In this model, the dynamics of the MP is given by,

$$C_m \frac{dV}{dt} = -g_L (V - E_L) - I_{Na} - I_{Kd} - I_M - A^{-1} I_{syn}, \quad (2)$$

with the current densities

$$I_{Na} = \overline{g}_{Na} m^3 h (V - E_{Na}) \quad (3)$$

$$I_{Kd} = \overline{g}_{Kd} n^4 (V - E_K)$$

$$I_M = \overline{g}_M p (V - E_K),$$

where C_m=1 μF/cm^2 is the specific membrane capacity, g_L=0.045 mS/cm^2 is the leak conductance density, and E_L=−80 mV is the leak reversal potential. I_{Na} is the voltage-dependent Na^+ current and I_{Kd} is the 'delayed-rectifier' K^+ current, which underlie the AP repolarisation. I_M is a non-inactivating K^+ current causing spike frequency adaptation and A is the total membrane area, which was 34636 μm^2. m, h, n, p are dynamical activation variables (for details see Destexhe et al., 1999).

The total synaptic current consists of excitatory and inhibitory parts:

(4) $$I_{syn} = g_e(t)(V - E_e) + g_I(t)(V - E_I),$$

with the reversal potentials E_e and E_I. The conductances $g_e(t)$ and $g_I(t)$ are Ornstein-Uhlenbeck processes with correlation times τ_e and τ_I.

To compare the AP onset dynamics between cortical neurons and the model in the presence of a fluctuating input (e.g. Fig. 1c, Fig. 2e,f), we used this model with exactly the same parameters as in the above paper.

Robustness against variations in model parameters and structure

By various modification of the models we tried to achieve a better match of recorded and simulated APs. As described in the subsequent sections, we modified the sodium current activation curve and the peak conductances, included various adaptation currents (Wang et al. 2003), replaced the simple mean channel kinetics with a stochastic dynamics of population of individual sodium channels (Schneidman et al. 1998), assessed the impact of state-dependent instead of voltage-dependent inactivation of sodium channels (Patlak et al. 1991). None of these modifications brought the model behaviour anywhere close to reproducing the two salient features of the recorded APs.

To study the impact of sodium channel activation on the AP initiation we modified the model described above by changing the Na-peak conductance $\bar{g}_{Na}$ (by factors of 2, 5, 10, 20) and the $m(t)$ activation curve, by changing its steepness by factors of 0.2, 0.5, 1.5, 2, 5, 10.

The m^3-term describing the activation of the sodium channels was replaced by the sodium activation curve measured by Huguenard et al. (1989), with the two parameters k and $V_{1/2}$:

(5) $$I_{Na} = \bar{g}_{Na}(1+\exp((-V+V_{1/2}+\Delta)/k)^{-1} n(t)(V-E_{Na})$$

We used combinations of k (changed by factors of 0.2, 0.5, 1.5, 2, 5, 10) and Δ (-10mV, -5mV, 6mV, 12mV, 20mV, 22mV) to change the AP onset rapidness while preserving a stationary firing rate of approximately 10Hz. In addition, the potassium peak conductance was changed by factors of 2 and 5 to assess its impact on the onset potential variability.

Model B: Adaptation currents and AP initiation (Wang et al.)

To assess the impact of adaptation currents on the response variability in Hodgkin-Huxley type models, we also implemented a two-compartmental model including adaptation currents developed by Wang et al. (2003).

The model has two compartments, one representing the soma and the initial segment (V_s) and the other representing the dendritic tree (V_d). The AP generating currents are located in the soma. High threshold Ca^{2+}, as well as Ca^{2+}-dependent K^+ currents are present in both compartments. In addition, the somatic compartment incorporates a slow Na^+-activated K^+ current.

The dynamics of the model is defined by the following differential equations:

(1) $C_m \frac{dV_s}{dt} = -I_L - I_{Na} - I_{Ca,s} - I_{KCa,s} - I_{KCa} - (g_c / p)(V_s - V_d) + I_{ext}(t)$

(2) $\frac{dh}{dt} = \phi_h(\alpha_h(V_s)(1-h) - \beta_h(V_s)h)$

(3) $\frac{dn}{dt} = \phi_n(\alpha_n(V_s)(1-n) - \beta_n(V_s)n)$

(4) $\frac{d[Ca^{2+}]_s}{dt} = -\alpha_{Ca,s} I_{Ca,s} - [Ca^{2+}]_s / \tau_{Ca,s}$

(5) $\frac{d[Na^+]}{dt} = -\alpha_{Na} I_{Na} - 3R_{pump}(\varphi_{Na}([Na^+]_{eq}))$

(6) $C_m \frac{dV_d}{dt} = -I_L - I_{Ca,d} - I_{KCa,d} - (g_c /(1-p))(V_d - V_s)$

(7) $\frac{d[Ca^{2+}]_d}{dt} = -\alpha_{Ca,d} I_{Ca,d} - [Ca^{2+}]_d / \tau_{Ca,d}$

The membrane capacity is denoted by $C_m = 1\mu F / cm^2$, the external current is $I_{ext}(t)$ and the leak current is $I_L = g_L(V - V_L)$. The coupling current between the soma and the dendrite is proportional to $V_d - V_s$, with the coupling conductance $g_c = 2\,\text{mS/cm}^2$. The parameter p=(somatic area/total area)=0.5. The maximum conductances are given by $g_L = 0.1$, $g_{Na} = 45$, $g_K = 18$, $g_{Ca,s} = g_{Ca,d} = 1$, $g_{KCa,s} = g_{KCa,d} = 5$, $g_{KNa} = 5\,\text{mS/cm}^2$. The reversal potentials are given by $V_L = -65$, $V_{Na} = 55$, $V_K = -80$, $V_{Ca} = 120\,\text{mV}$.

The sodium current in the somatic compartment is given by $I_{Na} = g_{Na} m_\infty{}^3(V_s) h (V_s - V_{Na})$ with $m_\infty(V_s) = \alpha_m /(\alpha_m + \beta_m)$, $\alpha_m(V) = -0.1(V+33)/(\exp(-0.1(V+33)))$ and $\beta_m(V) = 4\exp(-(V+58)/12)$. The inactivation variable h is described by $\alpha_h(V) = 0.07(\exp(-(V+50)/10))$ and $\beta_h(V) = 1/(\exp(-0.1(V+20))+1)$. The delayed rectifier is given by $I_K = g_K n^4 (V_s - V_K)$ with the activation variable n given by $\alpha_n(V) = -0.01(V+34)/(\exp(-0.1(V+34))-1)$ and

$\beta_n(V) = 0.125\exp(-(V+44)/25)$. The temperature factors are $\phi_h = \phi_n = 4$. The time constants are $\tau_x(V) = 1/(\alpha_x + \beta_x)$.

The high-threshold calcium current is given by $I_{Ca} = g_{Ca} v_\infty^{\,2}(V)(V - V_{Ca})$ with the activation variable $v_\infty(V) = 1/(1+\exp(-(V+20)/9))$. The voltage-independent, calcium activated potassium current is given by $I_{KCa}(V) = g_{KCa}([Ca^{2+}]_i/([Ca^{2+}]_i + K_D))(V - V_K)$, with $K_D = 30\,\mu$M. The intracellular calcium concentration $[Ca^{2+}]_i$ is assumed to be governed by a linear equation with α_{Ca} proportional to the ratio of the membrane area and the volume immediately beneath the membrane, $\alpha_{Ca} = 0.002\,\mu\text{M}(\text{ms}\mu\text{A})^{-1}\text{cm}^2$ in the dendritic compartment and $\alpha_{Ca} = 0.00067\,\mu\text{M}(\text{ms}\mu\text{A})^{-1}\text{cm}^2$ in the somatic compartment. The extrusion and buffering processes are described collectively by a first-order decay process with a time constant $\tau_{Ca} = 80\,\text{ms}$ in the dendrite and $\tau_{Ca} = 240\,\text{ms}$ in the soma.

The intracellular $[Na^+]_i$ concentration is incremented by Na^+ influx through I_{Na}. The Na^+-dependent K^+-current is determined by $I_{KNa} = g_{KNa}\omega_\infty([Na^+]_i)(V_s - V_K)$, with the activation function

(8) $$\omega_\infty([Na^+]_i) = \frac{P_{\max}}{1 + (EC_{50}/([Na^+]_i)^{n_H}}$$

$P_{\max} = 0.37$ defines the maximum opening probability of the channels, $EC_{50} = 38.7\text{mM}$ is the $[Na^+]_i$ for half activation and $n_H = 3.5$ is the Hill coefficient. The influx of $[Na^+]_i$ is controlled by $-\alpha_{Na} I_{Na}$ with $\alpha_{Na} = 3\cdot 10^{-4}\,\text{mM}$.

The extrusion of $[Na^+]_i$ by the ion pump was modelled as $-3R_{pump}(\varphi_{Na}([Na^+]_i) - \varphi([Na^+]_{eq})$, where $\varphi_{Na}(x) = x^3/(x^3 - K_p^{\,3})$, $K_p = 15\,\text{mM}$ and

$R_{pump} = 6 \cdot 10^{-4}$ mM/ms . The sodium concentration at the resting state is given by $[Na^+]_{eq} = 8\,\text{mM}$.

This model was driven by a fluctuating synaptic input current using the same point conductance model as in (Destexhe et al., 1999) and described above. The model was subsequently modified in the same way as the first model, i.e. the steepness of voltage-dependence of the activation was increased by factors of 0.2, 0.5, 1.5, 2, 5, 10 while preserving a stationary firing rate of approximately 10 Hz, by either changing the mean input current or shifting the activation curve as in Model A.
In both models, we simulated 5s long periods of neuronal activity, whereby in the second model, care was taken that the adaptation currents where statistically stationary. The simulated data were then analyzed using the same procedures as the experimentally obtained data.

All numerical simulations were performed in C++, all analyses were done using Matlab V6.5 (R13). For the numerical integration of the differential equation we used an Euler integration with an integration step of 10^{-3} ms .

Channel noise and AP initiation

In Hodgkin-Huxley type models, the ensemble dynamics of voltage-gated ion channels is described by products of continuous activation and inactivation variables which, in turn, are modelled as first order kinetics. Since natural membranes have a limited number of channels one expects MP fluctuations reflecting discrete channel opening and closing events (Chow & White 1996; Schneidman et al., 1998). Can this discrete switching explain the AP initiation observed in cortical neurons? To answer this question, it is instructive to first assess how many channels on average are involved in the generation of an AP. The conductance of a single voltage-gated

Na-channel is estimated to be on the order of $\gamma = 20$ pS (Neumcke & Stämpfli, 1982). From the total sodium current flowing through a patch of the membrane, the number of channels in a membrane area of size 200 µm² in a pyramidal cell has been estimated as approximately N = 12000, yielding a total conductance of 240 nS (Schneidman et al, 1998).

To assess if intrinsic channel noise can account for the AP initiation in cortical neurons, we implemented discrete Markov models, in which the opening and closing of individual sodium and potassium channels was simulated (Schneidman et al., 1998). The kinetic model for a population of sodium channels that reproduces the behaviour of a Hodgkin-Huxley type model for high channel densities is given by the following scheme (Patlak, 1991):

$$\begin{array}{ccccccc} & 3\alpha_m & & 2\alpha_m & & \alpha_m & \\ m_0h_1 & \rightleftharpoons & m_1h_1 & \rightleftharpoons & m_2h_1 & \rightleftharpoons & m_3h_1 \\ & \beta_m & & 2\beta_m & & 3\beta_m & \\ \alpha_h \updownarrow \beta_h & & \alpha_h \updownarrow \beta_h & & \alpha_h \updownarrow \beta_h & & \alpha_h \updownarrow \beta_h \\ & 3\alpha_m & & 2\alpha_m & & \alpha_m & \\ m_0h_0 & \rightleftharpoons & m_1h_0 & \rightleftharpoons & m_2h_0 & \rightleftharpoons & m_3h_0 \\ & \beta_m & & 2\beta_m & & 3\beta_m & \end{array}$$

In this description, each channel has 8 possible states and $\left[m_i h_j\right]$ is the number of channels that are in state $m_i h_j$. An individual channel is open, when it is in the state $m_3 h_1$, but closed in all other states. Thus, the total sodium membrane conductance is given by $g_{Na} = \gamma_{Na}[m_3 h_1]$.

The population of voltage-gated potassium channels is modelled by the following kinetic scheme:

$$\begin{array}{ccccccccc} & 4\alpha_n & & 3\alpha_n & & 2\alpha_n & & \alpha_n & \\ n_0 & \rightleftharpoons & n_1 & \rightleftharpoons & n_2 & \rightleftharpoons & n_3 & \rightleftharpoons & n_4 \\ & \beta_n & & 2\beta_n & & 3\beta_n & & 4\beta_n & \end{array}$$

Here, each channel has 5 possible states. A channel is open when it is in the state n_4.

The total potassium conductance is then given by $g_K = \gamma_K [n_4]$.

The rates α_x and β_x are the standard Hodgkin-Huxley transition rates (Hille, 2001).

In each time step Δt of the simulation, the number of channels Δn_{AB} that switch between states A and B with rate r is determined by choosing a random number from a binomial distribution:

$$(9)\ \mathrm{Prob}(\Delta n_{AB}) = \begin{pmatrix} n_A \\ \Delta n_{AB} \end{pmatrix} p^{\Delta n_{AB}} (1-p)^{(n_A - \Delta n_{AB})}$$

where n_A denotes the number of channels in state A and $p=r\Delta t$.

In Fig. 2SI, results of a simulation of 3 conductance-based models with the number of sodium channels equal to (12000), half (6000) and 10 times lower (1200) than the experimental estimate, and a fixed number of potassium channels (3600) are used. The same fluctuating current was injected into the three models. With a decreasing number of channels, the phase plot trajectories became noisier and the apparent variability of the onset potential larger, (B,D,F), but the steepness of the AP onsets did not change. With none of the three models, the AP onset dynamics matched the values for the onset rapidness and onset potential variability, observed in *in vivo* recordings.

The activation scheme described above is the kinetics that corresponds to the classical Hodgkin-Huxley model in the limit of high channel density and negligible stochastic fluctuations. This scheme, however, is known to incorrectly represent the inactivation of sodium channels, which is state-dependent rather than voltage-dependent (Hille, 2001). To test, the impact of state-dependent inactivation, we also implemented a scheme which includes more dynamical steps for activation and

inactivation (Patlak, 1991, Model 7). With none of the schemes tested, the AP onset rapidness substantially changed. Channel noise is thus not a plausible candidate to explain the AP onset dynamics observed *in vivo* (e.g. Fig. 2 in the paper).

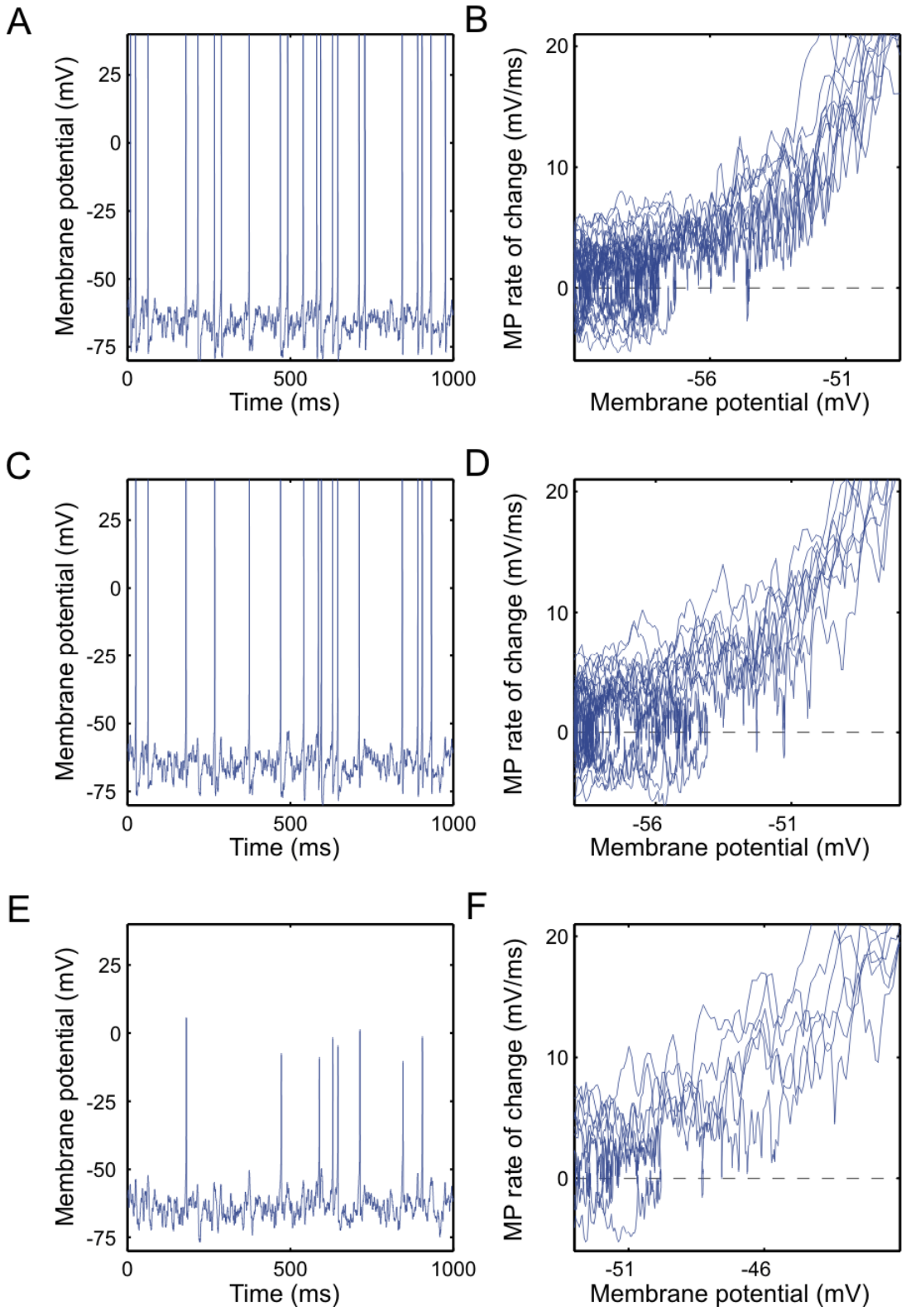

Fig 2SI: Impact of channel noise on the onset dynamics of APs in a conductance based neuron model. (A,C,E) Voltage trace of a model neuron with the same fluctuating synaptic background input and a different number of voltage-gated sodium channels (A: 12000, C: 6000, E: 1200) and 3600 potassium channels. (B,D,F): Corresponding phase plots. With a decreasing number of sodium channels the AP onset dynamics becomes noisier. Both, the AP onset span and the onset rapidness remain unaffected.

AP onset variability and steepness are antagonistic in Hodgkin-Huxley type models

In conductance based models, the dynamics of the MP $V(t)$ is given by:

$$(10) \qquad CdV(t)/dt = g_{Na}h(t)m(t)^3(V_{Na} - V(t)) + I_K + \cdots$$

Here C denotes the membrane capacity, g_{Na} the sodium channel peak conductance, $m(t)$ the sodium channel activation and $h(t)$ the inactivation. The activation and inactivation follow a first order kinetics, where the time constant of the activation $\tau_m(V)$ is typically on the order of 0.2ms and the inactivation time constant $\tau_h(V)$, as well as the time constants of all other channels, are typically much larger.

During the initial AP phase, the maximum rate of change of the MP can thus be estimated by replacing $m(t)$ by its steady state value $m_\infty(V)$ and replacing the inactivation variable by a constant h_0:

$$(11) \qquad dV(t)/dt \le I_0 + g_{Na}h_0 m_\infty{}^3(V)(V_{Na} - V(t))$$

Right at the AP onset, the sodium activation curve starts exponentially:

$$(12) \qquad \begin{aligned} m^3(V) &= (1+\exp(-(V-V_{1/2})/k))^{-1} \\ &\simeq \exp((V-V_{1/2})/k) \end{aligned}$$

A multiplication of $m^3(V)$ by a factor G is therefore equivalent to a shift of the whole curve by $k \log G$. For APs with a gradual onset ($k = 6$), a shift of 10mV would therefore require a 5-fold change in the effective sodium peak conductance, while for more rapid onsets ($k = 1$) it would require a 22000-fold change.

References

Chow CC, White JA. Spontaneous action potentials due to channel fluctuations. Biophys. J. 71, 3013-21 (1996)

Destexhe, A. & Paré, D., Impact of network activity on the integrative properties of neocortical pyramidal neurons *in vivo*. *J. Neurophysiol.* **81**, 1531–1547 (1999)

Hille, B. (2001). Ion Channels of Excitable Membranes. 3. Edition. (Sunderland, MA: Sinauer).

Huguenard, J.R., Hamill, O.P. & Prince, D.A. Sodium channels in dendrites of rat cortical pyramidal neurons. Proc. Natl. Acad. Sci. 86, 2473-2477 (1989).

Martina M, Jonas P. Functional differences in Na+ channel gating between fast-spiking interneurones and principal neurones of rat hippocampus. J. Physiol. 505, 593-603 (1997)

Neumcke, B. & Stämpfli, R.. Sodium currents and sodium-current fluctuations in rat myelinated nerve fibres. J. Physiol., 329, 163–184 (1982)

Patlak, J. Molecular kinetics of voltage-dependent Na+ channels. *Physiol. Rev.* 71, 1047-1080 (1991).

Schneidman, E., Freedman, B., & Segev, I. Ion channel stochasticity may be critical in determining the reliability and precision of spike timing. Neural. Comput., 10, 1679–1703 (1998)

Wang, X.J., Liu, Y., Sanchez-Vives, M.V. & McCormick, D.A., Adaptation and temporal decorrelation by single neurons in the primary visual cortex. J. Neurophysiol. 89, 3279-3293 (2003).

Unique features of action potential initiation in cortical neurons

Björn Naundorf, Fred Wolf, Maxim Volgushev

Online supplementary information (Part 3 of 3):

Cooperative channel activation

In this part of the Supplementary Information we introduce a model of AP initiation by cooperative activation of voltage-gated sodium channels and characterize its basic properties. Then we describe the computational consequences of the characteristic features of cortical action potential initiation. Using a novel phenomenological neuron model, we show that these features allow a neuronal population to encode rapidly varying signals and to suppress responses to slowly varying stimuli.

Contents

AP initiation with cooperative sodium channel activation 2

The single channel model 4

Mean field model of cooperative gating 5

The collective sodium activation curve 7

AP generation with cooperative sodium channels 8

Rate functions and parameters 8

Functional consequences of ‘anomalous’ AP initiation 10

AP initiation with cooperative sodium channel activation

The large AP onset rapidness typical of cortical APs suggests that during the initial phase of APs, sodium channels open in a coordinated fashion. To investigate whether cooperative sodium channel activation can quantitatively explain the co-occurrence of a large AP onset span and a large AP onset rapidness, we constructed and analysed a model for AP generation, in which sodium channel activation could be varied between independent and cooperative gating. In the model, individual sodium channels open (close) either independently of each other or cooperatively, i.e. the opening (closing) of one channel increases the probability of neighbouring sodium channels to also open (close). Our model is based on a model of single sodium channel gating introduced by Aldrich, Corey and Stevens (1983). The single channel model incorporates state-dependent inactivation from the open state, voltage-dependent inactivation from the closed state and is consistent with sodium channel activation curves and channel open times obtained from patch recordings (Aldrich, Corey and Stevens 1983; Martina and Jonas 1997). In the cooperative activation model, an individual channel i is coupled to K neighbouring channels such that the opening of each of them shifts the activation curve of channel i by a voltage shift $-J$ towards more hyperpolarized values. With $J = 0mV$, the model describes statistically independent single channel activation. With $J > 0mV$, channels are activating in a cooperative fashion. To model AP generation, mean field equations for the resulting sodium current were incorporated into the current balance equation of a membrane compartment. The compartment contained - besides the sodium channels - a large leak conductance. For simplicity, the model contains no voltage dependent potassium channels as their inclusion leaves the nature of AP onsets unaffected but complicates the analysis. In the following, we describe the

construction of the model and its main properties. As shown in the paper and below, (1) there is a critical coupling strength above which the current voltage relationship of an ensemble of sodium channels exhibits a step-like activation, deviating from the activation curve of an isolated channel. (2) In a neuronal membrane this leads to the generation of APs exhibiting a large onset rapidness. (3) Voltage-dependent inactivation from closed states and slow deinactivation of sodium channels lead to a large AP onset span. The model, thus does not exhibit an antagonism between AP onset rapidness and onset variability.

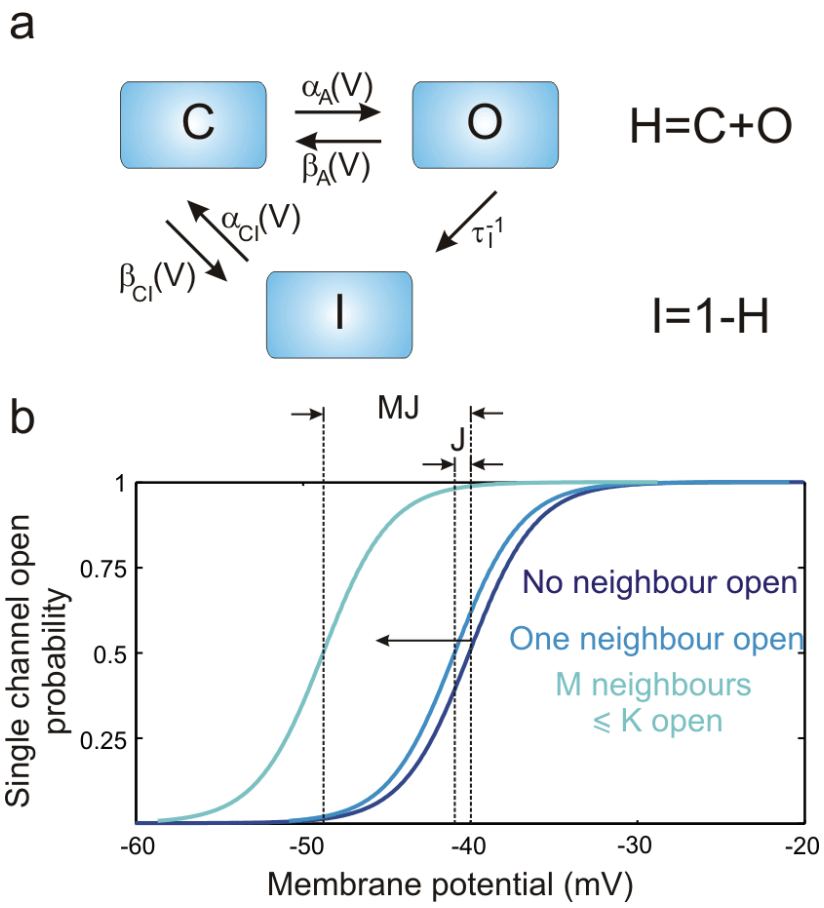

Figure 3SI (a) State transition scheme of the single sodium channel model. (b) Modelling inter-channel cooperativity: In the coupled model, the opening of neighbouring channels shifts the single channel activation curve to more hyperpolarized potentials such that the probability of channel opening at a given MP is increased.

The single channel model

Our model of cooperative sodium channel activation is based on a single channel model originally introduced by Aldrich, Corey and Stevens (1983). Its state transition scheme (Fig. 3SI a) has three states: *open*, *closed* and *inactivated* and incorporates three types of state transitions: voltage-dependent activation and deactivation, voltage-independent inactivation from the open state, and voltage-dependent

inactivation from the closed state and de-inactivation from the inactivated to the closed state.

Voltage-independent inactivation from the open state occurs with rate τ_I^{-1}.

Transitions between closed and open states and between inactivated and closed states occur with rates $\alpha_A(V)$ (opening), $\beta_A(V)$ (closing) and $\alpha_{CI}(V)$ (de-inactivation), $\beta_{CI}(V)$ (inactivation), respectively (Fig. 3SI a). The dynamics of a population of such channels is described by kinetic equations for the fraction of open channels $O(t)$ and the fraction of available channels $H(t)$

$$\dot{O}(t) = \alpha_A(V)\big(H(t) - O(t)\big) - \big(\tau_I^{-1} + \beta_A(V)\big)O(t)$$
$$\dot{H}(t) = \alpha_{CI}(V)\big(1 - H(t)\big) - \beta_{CI}(V)\big(H(t) - O(t)\big) - \tau_I^{-1}O(t)$$

For discussing model properties it is useful to consider two characteristic functions: The instantaneous single channel activation curve, $o_\infty(V)$ and the equilibrium inactivation function $I_\infty(V)$. If the time scale of activation is shorter than the inactivation time constant τ_I, the activation of channels from the available fraction, $H(t)$, is described by the instantaneous single channel activation curve

(13) $$o_\infty(V) = \alpha_A(V) / \big(\alpha_A(V) + \beta_A(V)\big).$$

For constant membrane potential and negligible sodium channel activation, the equilibrium inactivation function

(14) $$I_\infty(V) = \beta_{CI}(V) / \big(\alpha_{CI}(V) + \beta_{CI}(V)\big)$$

describes the equilibrium fraction of inactivated channels as a function of membrane potential.

Mean field model of cooperative gating

Based on the above model of single channel gating we formulated a mean field model of cooperative sodium channel activation. To derive this model, we assumed that each channel is coupled to K neighbouring channels. Opening of any of these neighbours is then assumed to cause a shift of the instantaneous activation curve of the channel by $-J$ towards lower membrane potentials. The activation and deactivation rates of channel i are then,

$$\begin{aligned} \alpha_i^A(V) &= \alpha_A(V + \sum_j J_{ij}\sigma_j) \\ \beta_i^A(V) &= \beta_A(V + \sum_j J_{ij}\sigma_j) \end{aligned} \tag{15}$$

where $J_{ij} = J$ if channels i and j are coupled, $J_{ij} = 0$ else, and σ_j is a binary single channel state variable labelling channels in the open state: $\sigma_j = 1(0)$ if channel j is open (not open). A mean field model of cooperative channel gating is obtained by replacing the voltage shift term $\sum_j J_{ij}\sigma_j$ by its population average $KJO(t)$. The dynamics of the open and available fractions are then,

$$\begin{aligned} \dot{O}(t) &= \alpha_A(V + KJO(t))\big(H(t) - O(t)\big) - \big(\tau_I^{-1} + \beta_A(V + KJO(t))\big)O(t) \\ \dot{H}(t) &= \alpha_{CI}(V)\big(1 - H(t)\big) - \beta_{CI}(V)\big(H(t) - O(t)\big) - \tau_I^{-1}O(t) \end{aligned} \tag{16}$$

.

The case of independent gating is recovered if the coupling strength is set to zero, $J = 0$. For $J > 0$, the cooperative case, the dynamics of the open and available fraction does not passively follow the voltage time-course but contains a positive feedback interaction between sodium channels.

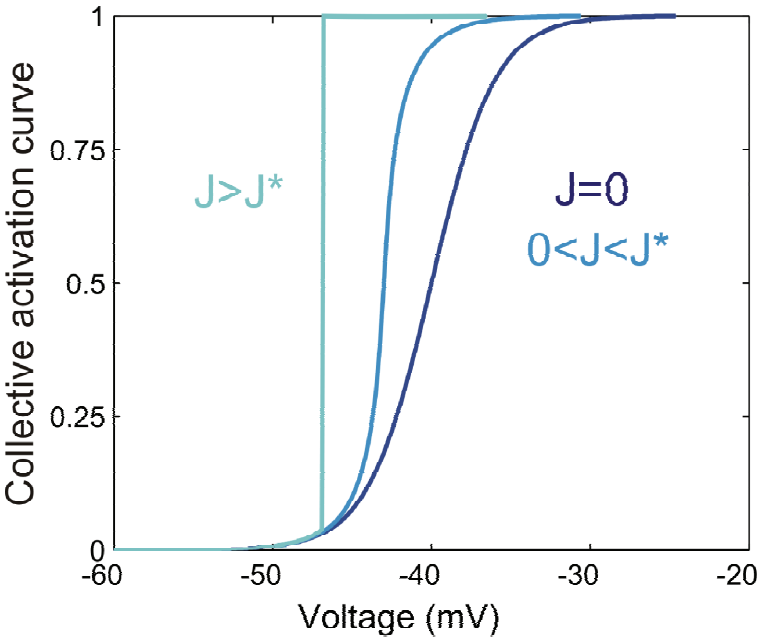

Figure 4SI: Schematic representation of the collective activation curves of sodium channels for varying degrees of inter-channel coupling.

The collective sodium activation curve

The impact of cooperative gating is revealed by considering the fraction of open sodium channels relative to the available fraction, as a function of the MP for $\tau_I^{-1} = 0$, subsequently called the *collective sodium activation curve*. Assuming a temporally constant available fraction H_0, the collective sodium activation curve satisfies the equation

(17) $$o_\infty^J(V) = o_\infty(V + H_0 K J o_\infty^J(V)),$$

where $o_\infty(V)$ is the instantaneous activation curve of independent channels. This equation is a self-consistency relation for $o_\infty^J(V)$. In the uncoupled case, $J = 0$, the collective sodium activation curve equals the single channel activation curve. For $J > 0$, the collective sodium activation curve $o_\infty^J(V)$ becomes progressively steeper than $o_\infty(V)$ with increasing values of J and develops a discontinuous jump at a critical potential V^* when the coupling strength J becomes larger than a critical

value J^* (Fig. 4SI). This means that for a supercritical coupling $J > J^*$, a small increase in MP can cause the opening of a macroscopically large fraction of sodium channels, indicating a phase transition in the collective behaviour of the population of channels.

AP generation with cooperative sodium channels

To study the impact of cooperative sodium channel activation on the generation of APs we incorporated the current mediated by the population of coupled sodium channels, $I_{Na}(t) = g_{Na} O(t)\left(V_{NA} - V(t)\right)$, where g_{Na} is the sodium peak conductance, and V_{Na} the sodium current reversal potential, and a leak current $I_L(t) = g_L\left(V_L - V(t)\right)$, with the leak conductance g_L and the reversal potential V_L, into the current balance equation for a membrane compartment of capacitance C_M. We simulated this system driven by a fluctuating input current which was modelled by an Ornstein-Uhlenbeck process. The dynamics of the compartment is described by the following system of differential equations:

$$
\begin{aligned}
&\tau\, \dot{z}(t) = -z(t) + \sqrt{\tau}\eta(t) \\
&c_M \dot{V}(t) = g_L\left(V_L - V(t)\right) + g_{Na} O(t)\left(V_{NA} - V(t)\right) + I_0 + \sigma z(t) \\
&\dot{O}(t) = \alpha_A(V + KJO(t))\left(H(t) - O(t)\right) - \left(\tau_I^{-1} + \beta_A(V + KJO(t))\right)O(t) \\
&\dot{H}(t) = \alpha_{CI}(V)\left(1 - H(t)\right) - \beta_{CI}(V)\left(H(t) - O(t)\right) - \tau_I^{-1} O(t)
\end{aligned}
\qquad (20)
$$

where τ is the correlation time of the input current, I_0 its average value, and σ its standard deviation.

Rate functions and parameters

The rate functions describing individual sodium channel activation / deactivation and inactivation / deinactivation where chosen as,

$$
\begin{aligned}
\alpha_A(V) &= \tau_A^{-1}\left(1+\exp\left(-\left(V-V_{1/2}^A\right)/k^A\right)\right)^{-1} \\
\beta_A(V) &= \tau_A^{-1}\left(1+\exp\left(\left(V-V_{1/2}^A\right)/k^A\right)\right)^{-1} \\
\alpha_{CI}(V) &= \tau_{CI}^{-1}\left(1+\exp\left(-\left(V-V_{1/2}^{CI}\right)/k^{CI}\right)\right) \\
\beta_{CI}(V) &= \tau_{CI}^{-1}\left(1+\exp\left(\left(V-V_{1/2}^{CI}\right)/k^{CI}\right)\right)
\end{aligned}
\tag{21}
$$

With this choice the instantaneous single channel activation curve, and the equilibrium inactivation function are of sigmoidal shape

$$
\begin{aligned}
o_\infty^A(V) &= \left(1+\exp\left(\left(V-V_{1/2}^A\right)/k^A\right)\right)^{-1} \\
I_\infty(V) &= \left(1+\exp\left(\left(V-V_{1/2}^{CI}\right)/k^{CI}\right)\right)^{-1}
\end{aligned}
\tag{22}
$$

and the relaxation times for the two transitions (considered independently) are voltage-independent constants τ_A and τ_{CI}.

Figure 5 of the paper shows numerical simulations of the model for parameter values

$V_{1/2}^A = -35mV, k^A = 6mV, \tau_A = 0.1ms, \tau_I = 0.5ms, V_{1/2}^{CI} = 80mV, k^{CI} = 4mV, \tau_{CI} = 30mV$

of the uncoupled activation dynamics and

$\tau = 50ms, C_M = 1\mu F/cm^2, g_L = 2mS/cm^2, V_L = -80mV, g_{Na} = 68.4mS/cm^2, V_{Na} = 50mV,$
$I_0 = 0\mu A/cm^2, \sigma = 12\mu A/cm^2$
of the currents and conductances.

With these parameters, the single channel activation curve is consistent with results obtained from patch recordings. Inactivation from the closed state has a broad voltage dependence and a relatively large timescale, leading to substantial fluctuation of the level of inactivation even in the absence of AP activity. For Fig. 5a, the coupling strength was chosen supercritical $J = 3.2mV, K = 1000$ leading to a discontinuous current voltage relationship. In Figure 5 of the paper, numerical simulations of the model obtained for these parameters are compared to simulations without cooperativity $J = 0$ (Fig.5b), and with a fast and voltage-independent

deinactivation and inactivation from the closed state $J = 0, \tau_{CI} = 4ms, V_{1/2}^{CI} = 80mV$ (Fig.5c).

The impact of the coupling on the onset potential variability is depicted in Fig. 5SI. The AP onset potential variability is determined by the available fraction of channels.

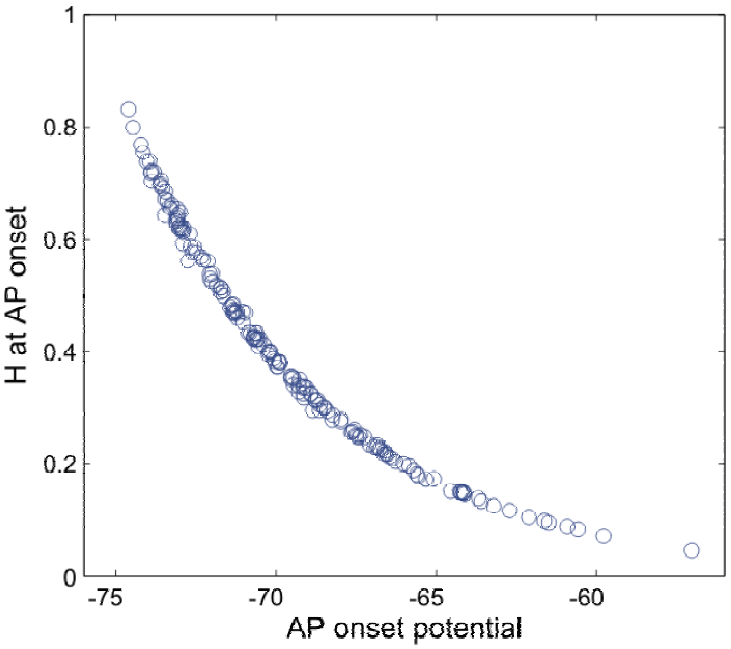

Fig 5SI: Impact of the channel coupling on onset potential variability. The AP onset potential is determined by the available fraction of channels *H*.

Functional consequences of 'anomalous' AP initiation

To understand the functional implications of a sharp AP onset in combination with a variable onset potential we formulated a phenomenological neuron model capturing the salient features of cortical AP initiation and analyzed its dynamical response properties when driven by fluctuating inputs. We idealized the rapid onset of APs at variable onset potentials by assuming that an AP is initiated instantaneously when the MP reaches a time-dependent threshold potential. The dynamics of the threshold potential was constructed to reproduce a key feature of the statistics of AP onset potentials: A large fraction of the AP onset variability is explained by a correlation between the onset potential and the mean MP preceding an AP (Henze & Buzsaki,

2001, Azouz &Gray 2003). The model shows that the large and history dependent fluctuations in AP onset potential equip a neuron with high pass filter characteristics and therefore with a very effective way of suppressing responses to slowly varying inputs.

The phenomenological model has two degrees of freedom: The MP $V(t)$ and a time-dependent firing threshold $\theta(t)$. The MP consists of two components: A Gaussian stochastic process $u(t)$ with the properties:

$$(23)\ \langle u(t)\rangle = V_0,\ \langle u(t)^2\rangle = {\sigma_V}^2,$$
$$(24)\ \langle \dot{u}(t)\rangle = 0,\ \langle \dot{u}(t)^2\rangle = {\sigma_{\dot{V}}}^2,$$

where the dots denote the first temporal derivative. The second part is a low-pass filtered time dependent signal $f(t)$, where the filter frequency is given by the inverse relaxation time constant of the membrane τ_M:

$$(25)\qquad \tau_M \dot{f}(t) = -f(t) + Signal(t)$$

Each time the MP crosses the threshold $\theta(t)$ from below, i.e. with a rate of change $\dot{V}(t) > 0$, a spike is emitted. Because in the regime considered here, the correlation time is much shorter than the mean time between two adjacent APs, we didn't incorporate an explicit afterhyperpolarization into the model.
The dynamics of the threshold is modelled by a first order kinetics, driven by the MP $V(t)$ with a time constant τ_θ:

(26) $\tau_\theta \dot{\theta} = (\theta_0 - \theta) + c(V(t) - V_0)$

where θ_0 is the threshold voltage and c the coupling between the threshold and the MP. Since we model the MP as a stochastic process, we will consider in the following an ensemble of such neurons and ensemble averaged quantities. For each neuron in this ensemble the MP fluctuations are independent, every neuron, however, receives the same input $f(t)$. The coding of this input by the ensemble averaged firing rate is the quantity studied.

The average number of APs in the ensemble of neurons in a time interval $(t, t + \Delta t)$ is given by:

(27) $\langle N \rangle = \left\langle \int_t^{t+\Delta t} dt' \delta(u(t') - \theta(t')) \left|\dot{u}(t')\right| \Theta(\dot{u}(t')) \right\rangle$

(28) $= \int_t^{t+\Delta t} dt' \left\langle \delta(u(t') - \theta(t')) \left|\dot{u}(t')\right| \Theta(\dot{u}(t')) \right\rangle$

(29) $= \int_t^{t+\Delta t} dt' \nu(t'),$

where the angular brackets $\langle \bullet \rangle$ denote the average over the ensemble. In the last equation we have introduced the time dependent firing rate $\nu(t)$, which is thus given by:

(30) $\nu(t) = \int_{-\infty}^{\infty} du(t)\, d\dot{u}(t)\, \delta(u(t) - \theta(t)) \left|\dot{u}(t)\right| \Theta(\dot{u}(t))\, P(u(t), \dot{u}(t) \mid t)$

Here $\delta(\bullet)$ denotes the Dirac distribution, $\Theta(\bullet)$ is the Heaviside function and the dots denote the first temporal derivatives. The time dependent joint probability density of

$u(t)$ and $\dot{u}(t)$ at time t, $P(u(t),\dot{u}(t)\,|\,t)$, is given by:

$$(31)\quad P(u(t),\dot{u}(t)\,|\,t) = (2\pi\sigma_V\sigma_{\dot{V}})^{-1}\exp\left\{-\frac{1}{2}\left(\frac{u(t)+f(t)}{{\sigma_V}^2}+\frac{\dot{u}(t)+\dot{f}(t)}{{\sigma_{\dot{V}}}^2}\right)\right\}$$

To study the response of the model to dynamically changing inputs, we assumed that the time dependent input signal is given by a cosine with amplitude A and frequency ω. The function $f(t)$ is then given as:

$$(32)\quad f(t) = \frac{A{\tau_M}^{-2}}{{\tau_M}^{-2}+\omega^2}\left(\cos(\omega t)+\tau_M\omega\sin(\omega t)\right)$$

Since the threshold time constant τ_θ is typically much larger than the membrane time constant, the threshold dynamics is approximated by:

$$(33)\quad \theta(t) = Ak\tau_M\frac{(1-\tau_M\tau_\theta\omega^2)\cos(\omega t)+(\tau_M+\tau_\theta)\omega\sin(\omega t)}{(1+{\tau_M}^2\omega^2)(1+{\tau_\theta}^2\omega^2)}+\theta_0$$

Evaluating the integral in Eq. (30) with this approximation we obtain an expression for the time dependent firing rate:

(34)

$$\nu(t) = (2\pi\sigma_V)^{-1}\exp\left(-\frac{(f(t)-\theta(t))^2}{2{\sigma_V}^2}\right)\left\{\sigma_{\dot{V}}\exp\left(-\frac{\dot{f}(t)^2}{2{\sigma_{\dot{V}}}^2}\right)+\sqrt{\frac{\pi}{2}}\dot{f}(t)(1+\mathrm{erf}(\dot{f}(t)/(\sqrt{2}\sigma_{\dot{V}}))\right\}$$

To study the response for small values of A we expand $\nu(t)$ in powers of A, giving the rate modulation in linear response approximation:

$$(35)\quad \nu(t) = \nu_0 + A\nu_1(\omega)\cos(\omega t + \varphi) + O(A^2),$$

with:

$$(36)\qquad \nu_0 = \frac{\sigma_V}{2\pi\sigma_{\dot V}}\exp\left(-\frac{\theta_0^{\,2}}{2\sigma_V^{\,2}}\right)$$

$$(37)\quad \nu_1(\omega) = \exp\left(-\frac{\theta_0^{\,2}}{2\sigma_V^{\,2}}\right)\frac{\left(\pi\omega^2(1+\tau_\theta^{\,2}\omega^2)\sigma_V^{\,4} + 2\theta_0\sigma_{\dot V}(\sqrt{2\pi}c\tau_\theta\omega^2\sigma_V^{\,2} + \theta_0((k-1)^2 + \tau_\theta^{\,2}\omega^2)\sigma_{\dot V})\right)^{1/2}}{\sqrt{8}\pi\sigma_V^{\,3}\left((1+\tau_M^{\,2}\omega^2)(1+\tau_\theta^{\,2}\omega^2)\right)^{1/2}}$$

$$(38)\quad \varphi(\omega) = \arctan\left(-\frac{\omega(\sqrt{2\pi}(1+\tau_\theta^{\,2}\omega^2)\sigma_V^{\,2} + 2\theta_0(k\tau_\theta + \tau_M(c-1-\tau_\theta\omega^2))\sigma_{\dot V})}{\sqrt{2\pi}\tau_M\omega^2(1+\tau_\theta^{\,2}\omega^2)\sigma_V^{\,2} + 2\theta_0(1-c+\tau_\theta(k\tau_M+\tau_\theta)\omega^2)\sigma_{\dot V}}\right)$$

In the limit $\omega \to \infty$, the amplitude of the rate modulation $\nu_1(\omega)$ becomes constant and independent of c:

$$(39)\quad \nu_1(\omega\to\infty) = (\sqrt{8}\pi\tau_M\sigma_V)^{-1}\exp\left(-\frac{\theta_0^{\,2}}{2\sigma_V^{\,2}}\right),$$

the phase lag $\varphi(\omega \to \infty)$ goes to zero.

This means, that even for very high stimulation frequencies, the model will respond to the input with a finite amplitude of the firing rate response, although the amplitude of $f(t)$ and $\theta(t)$ approaches zero for $\omega \to \infty$. This apparently counterintuitive result can be understood from the equation for the instantaneous firing rate (Eq. 34). It does not only incorporate the functions $f(t)$ and $\theta(t)$, but also the temporal

derivative $\dot{f}(t)$ which has a finite high-frequency limit. The finite high-frequency limit of the response function reflects the idealization of a sharp AP threshold, i.e. AP initiation with infinite AP onset rapidness. Models with finite AP onset rapidness in general exhibit a cut-off frequency, which depends on AP onset rapidness and increases when AP onset rapidness is increased (Fig. 6SI; Fourcaud 2003, Naundorf et al., 2005).

In the limit $\omega \to 0$, $\nu_1(\omega)$ is given by:

(40) $\nu_1(0) = \sqrt{2/\pi}(c-1)\frac{\theta_0 \tau_M \sigma_{\dot{V}}}{{\sigma_V}^2}\nu_1(\infty)$,

and the phase lag $\varphi(0)$ is zero.

These results show that the suppression of slowly varying inputs by the threshold variability in combination with the facilitation of the response at high frequencies by a high onset rapidness, equips a neuron model with high-pass filter characteristics. It is important to note that at low-frequencies, the amplitude of the rate modulation decreases with an increasing coupling constant c and becomes zero for $c = 1$, i.e. when the threshold is completely coupled to the mean modulation of the MP (Figure 7SI). In this regime, responses to slowly varying inputs are suppressed without a firing response. This behaviour qualitatively differs from the type of high-pass filter characteristic induced by AP-driven spike frequency adaptation (Benda and Herz 2003). With spike frequency adaptation, slowly varying inputs are never completely suppressed (see Eq.5.2 in Benda and Herz 2003).

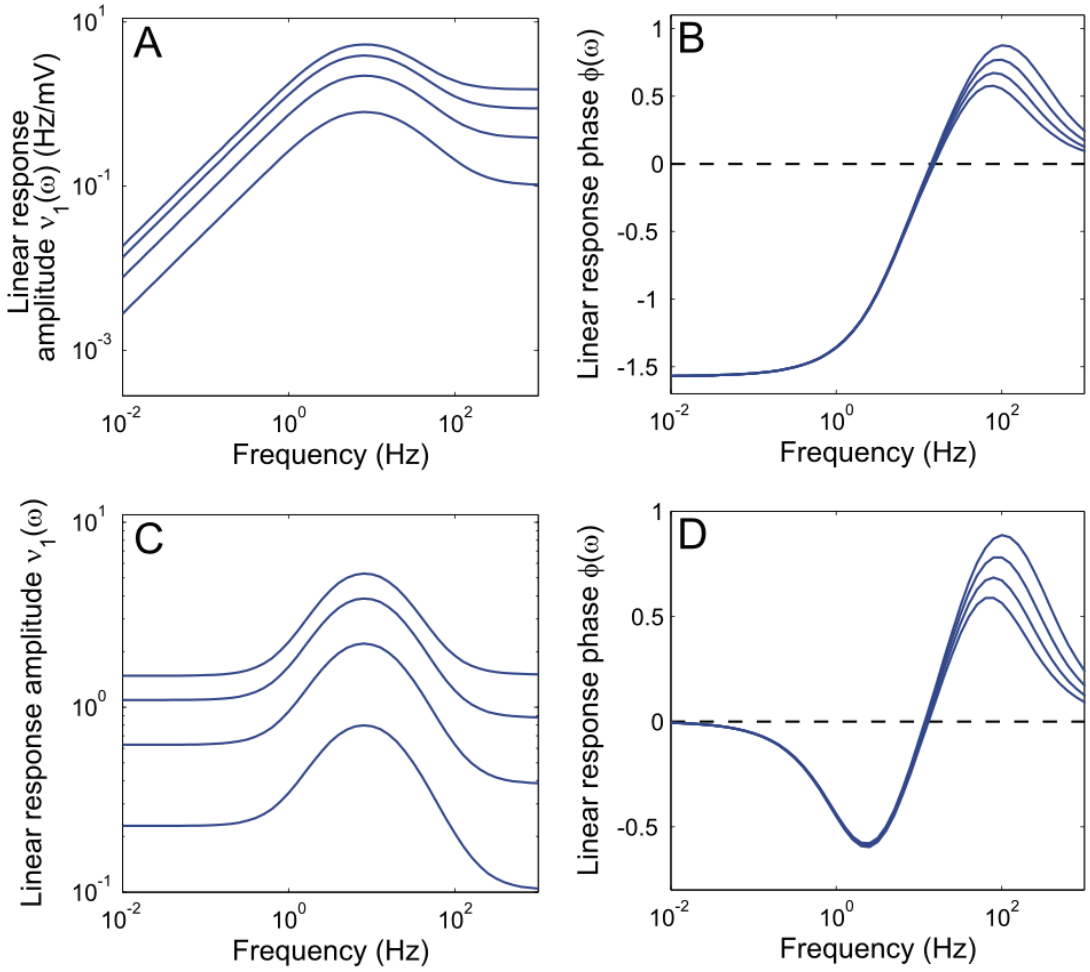

Fig 6SI: Linear response transfer function and phase shift of the $V-\psi$ model. (A) Transmission amplitude $\nu_1(\omega)$ and (B) phase for the case of a fully coupled threshold ($c = 1$) and different stationary firing rates (1 Hz, 5 Hz, 15 Hz, 30 Hz). (C,D) Transmission amplitude and phase for a partially coupled threshold (c=0.75). The transfer functions exhibit a pronounced resonance and settle on a finite value for $\omega \to \infty$. For the case of a fully coupled threshold, the transfer function goes to zero for $\omega \to 0$. Parameters:

$\sigma_V = 1.5, 1.75, 2.0, 2.25\text{mV}$, $\sigma_{\text{dV/dt}} = 1\text{mV/ms}$, $\tau_\psi = 30\text{ms}$, $\psi_0 = 5\text{mV}$.

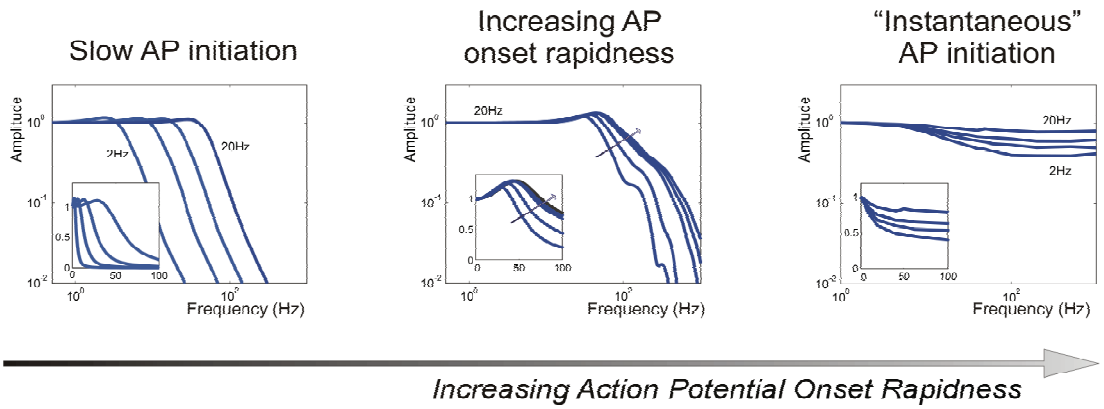

Fig 7SI: Effect of increasing the AP onset rapidness. With increasing onset rapidness, the transmission function shifts to larger values irrespective of the stationary firing rate. For the case of an instantaneous AP onset dynamics (fixed threshold), the transfer function remains finite in the limit $\omega \to \infty$. Curves are labelled for different stationary firing rates. (For details see Naundorf et al., 2005)

References

Aldrich R..W, Corey D.P., Stevens C.F. A reinterpretation of mammalian sodium channel gating based on single channel recording. *Nature* 306, 436-441 (1983)

Azouz, R., Gray, C.M. Adaptive coincidence detection and dynamic gain control in visual cortical neurons *in vivo*. *Neuron* 37, 513-532 (2003).

Benda J, Herz AV. A universal model for spike-frequency adaptation. Neural Comput. 15, 2523-64 (2003).

Fourcaud-Trocmé, N., Hansel, D., van Vreeswijk, C. & Brunel, N. How spike generation mechanisms determine the neuronal response to fluctuating inputs. *J. Neurosci.* 23, 11628-11640 (2003).

Henze, D.A. & Buzsaki, G. Action potential threshold of hippocampal pyramidal cells in vivo is increased by recent spiking activity. Neurosci. 105, 121-130 (2001).

Martina M, Jonas P. Functional differences in Na+ channel gating between fast-spiking interneurones and principal neurones of rat hippocampus. J Physiol. 505, 593-603 (1997)

Naundorf, B., Geisel T., Wolf F. Action Potential Onset Dynamics and the Response Speed of Neuronal Populations. *J. Comp. Neurosci.* 18, 297-309 (2005).

NEUROPHYSIOLOGY

Hodgkin and Huxley model — still standing?

Arising from: B. Naundorf, F. Wolf & M. Volgushev *Nature* **440,** 1060–1063 (2006)

Action potentials in cortical neurons show a variable threshold and a sudden rise in membrane potential at initiation. Naundorf *et al.*[1] fail to explain these features using single- or double-compartment Hodgkin–Huxley-style models, suggesting instead that they could arise from cooperative opening of Na^+ channels, although there is no direct biological evidence to support this. Here we show that these so-called unique features are to be expected from Hodgkin–Huxley models if the spatial geometry and spike initiation properties of cortical neurons are taken into account — it is therefore unnecessary to invoke exotic channel-gating properties as an explanation.

Cortical pyramidal cells initiate spikes in the axon initial segment (AIS) about 30–60 μm from their soma. These spikes then propagate antidromically through the soma and dendrites[2–4]. A well known feature of antidromic spikes is their sudden rise from baseline[5]. These critical properties were not considered by Naundorf *et al.*[1].

We made simultaneous whole-cell recordings from the AIS by patching the cut end of the axon (Fig. 1, legend) and the soma of layer-5 pyramidal neurons *in vitro*[6] during spontaneous spike generation (Fig. 1). Somatic spikes showed a rapid rise, or 'kink', at initiation (Fig. 1a, b) and the slope of the phase plot of spike dV/dt versus V at $dV/dt = 15\ mV\ ms^{-1}$ was $25 \pm 6.8\ ms^{-1}$ (mean ± s.d.; $n = 32$). The phase plots of dV/dt versus V typically revealed a biphasic rise, which was suggestive of two underlying components (Fig. 1b; $n = 30/32$), as observed in many cell types[7,8]. This biphasic component was not evident in the recordings of Naundorf *et al.*[1], although the low peak dV/dt of their recordings indicates that their spikes may not have been fully represented.

Intrasomatic injection of a noisy conductance that mimics the arrival of excitatory and inhibitory synaptic activity[9] resulted in significant variation in the apparent spike threshold ($n = 6$; Fig. 1c, green lines), as observed in the recordings of Naundorf *et al.*[1].

In contrast to somatic spikes, those recorded at the site of spike initiation, the AIS, showed a slower rise ($n = 10$; Fig. 1d, e). The slope of the phase plot of spike dV/dt versus V at $dV/dt = 15\ mV\ ms^{-1}$ was much lower for the AIS ($3.8 \pm 1.7\ ms^{-1}$; $n = 6$; $P<0.01$; Fig. 1d, e) than it was for the soma (Fig. 1a, b). The slow rise at spike initiation in the AIS is not an artefact of our method of axonal recording (Fig. 1, legend). On intrasomatic injection of a noisy conductance that mimics synaptic activity[9], the apparent spike threshold was less variable for the AIS ($n = 6$; Fig. 1f, green lines) than it was for the soma (Fig. 1c).

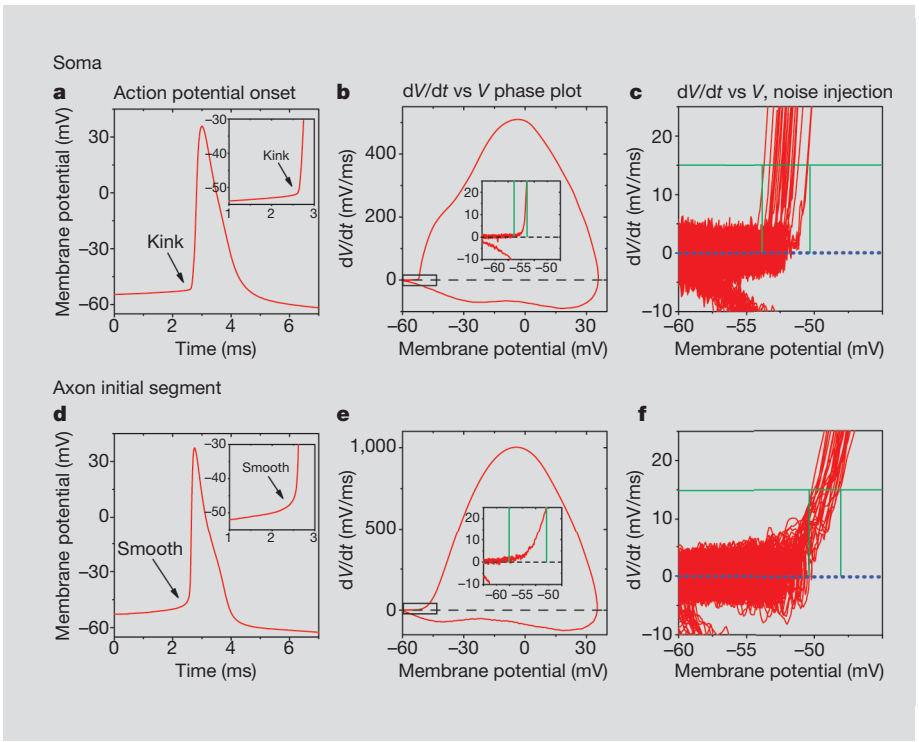

Figure 1 | Properties of spike initiation in the soma and axon of cortical pyramidal cells. a, Somatic spike exhibits a 'kink' at its onset. **b,** Phase plot (dV/dt versus V) and close-up of rapid initiation (inset) of the spike shown in **a**. **c,** Close-up of the phase plot of somatic spike initiation during noisy intrasomatic current injection[9], showing a broad distribution of thresholds (green lines). **d,** Whole-cell axonal recording (50 μm from the soma). **e,** Phase plot of the axonal spike. Note the smoothly rising dV/dt. **f,** Overlay of dV/dt versus V for the onset of axonal spikes, showing lower variability (compare with the soma) of spike threshold (green lines).
Methods. Simultaneous axonal and somatic whole-cell recordings were obtained with the multiclamp 700B amplifier from ferret prefrontal cortical layer-5 pyramidal cells in slices maintained *in vitro* at 36 °C (ref. 6). Spikes shown in **a**, **d**, as well as in **c**, **f**, were recorded simultaneously. Spikes occurred either during spontaneous synaptic activity[6] or in response to the intrasomatic injection of a noisy (10–15 mV) current injection[9]. Whole-cell axonal recordings obtained through patching the cut end of the axon (terminal bleb) do not result in abnormal smoothness of spikes because spikes recorded from distal (> 100 μm) axonal sites also show an onset kink owing to spike propagation (see also www.mccormicklab.org).

Spike initiation in the AIS is mediated by either a high Na^+-channel density in the AIS, as indicated by immunocytochemistry[10,11], or by a lesser density of Na^+ channels, which have a low threshold for activation[12]. Using a previous model of spike initiation in a layer-5 cortical pyramidal cell[13], we adjusted the axonal and somatic densities of Na^+ and K^+ channels until the spike waveform and its derivative were similar to those of our actual recordings (compare Figs 1 and 2).

Our Hodgkin–Huxley model initiated spikes in the AIS that then propagated antidromically through the soma and dendrites, as in real pyramidal cells. At the soma, these spikes showed a rapid rise at initiation (Fig. 2a, b), and the slope of the phase plot for spike initiation at $dV/dt = 15\ mV\ ms^{-1}$ was $21\ ms^{-1}$. Intrasomatic injection of artificial synaptic barrages[9] into the modelled neuron revealed a high variability of apparent spike threshold in the soma (Fig. 2c).

As in the whole-cell recordings, the rise in the model spike at initiation was smoother at the AIS (Fig. 2d, e) than at the soma (Fig. 2a, b). The slope of the phase plot for spike initiation at $dV/dt = 15\ mV\ ms^{-1}$ was considerably lower for the model AIS ($4\ ms^{-1}$) than for the soma, and both were in the range observed in normal cells. Intrasomatic injection of artificial synaptic barrages[9] showed a less variable threshold in

the AIS (Fig. 2f) than in the soma (Fig. 2c), as we found for real neurons (Fig. 1c, f).

We found that several other Hodgkin–Huxley models of cortical pyramidal cells, even one based on a relatively low density of Na^+ conductance in the axon, replicated the 'kink' and variability of somatic spikes (Fig. 2 legend). These features of spike initiation in the soma were dependent on the initiation of spikes in the AIS: increasing the somatic Na^+ conductance to a high level (7.5 nS μm^{-2}) and removing Na^+ conductance from the axon in the model presented here resulted in a loss of the kink at the foot of the spike (soma slope, 4.1 ms^{-1}) and a reduction in spike threshold variability in the soma (results not shown).

Our findings reveal that leading Hodgkin–Huxley models of cortical pyramidal cell spike initiation capture the so-called unique features observed by Naundorf *et al.*[1]. We attribute these features simply to recording from a site that is distant from the site of spike initiation and to the non-uniform distribution of spike properties over the somatic and axonal membrane. The initiation of spikes in the axon that then back-propagate into the soma can result in a rapid change in membrane potential (the kink) at the foot of the somatic spike. The large current supplied by the axonal spike precedes and overlaps with the current supplied by the local generation of the action potential in the soma during the rising phase of the spike. This results in a more rapid rise at the foot of the spike in the soma than would occur if there were no preceding spike in the axon. The apparent high threshold variability with intrasomatic recordings merely results from membrane potential differences between the soma and the actual site of spike initiation, the axon, at the time that spikes are generated. These membrane-potential differences arise from local electrophysiological differences, as well as spatial non-uniformity in synaptic activity. We conclude that the observations made by Naundorf *et al.*[1] are predictable by Hodgkin–Huxley theory and the known physiology of spike initiation[2–4], and that there is no need to invoke exotic interchannel cooperativity to explain their observations.

David A. McCormick*, Yousheng Shu*†, Yuguo Yu*

*Department of Neurobiology, Kavli Institute for Neuroscience, Yale University School of Medicine, New Haven, Connecticut 06510, USA
e-mail: david.mccormick@yale.edu

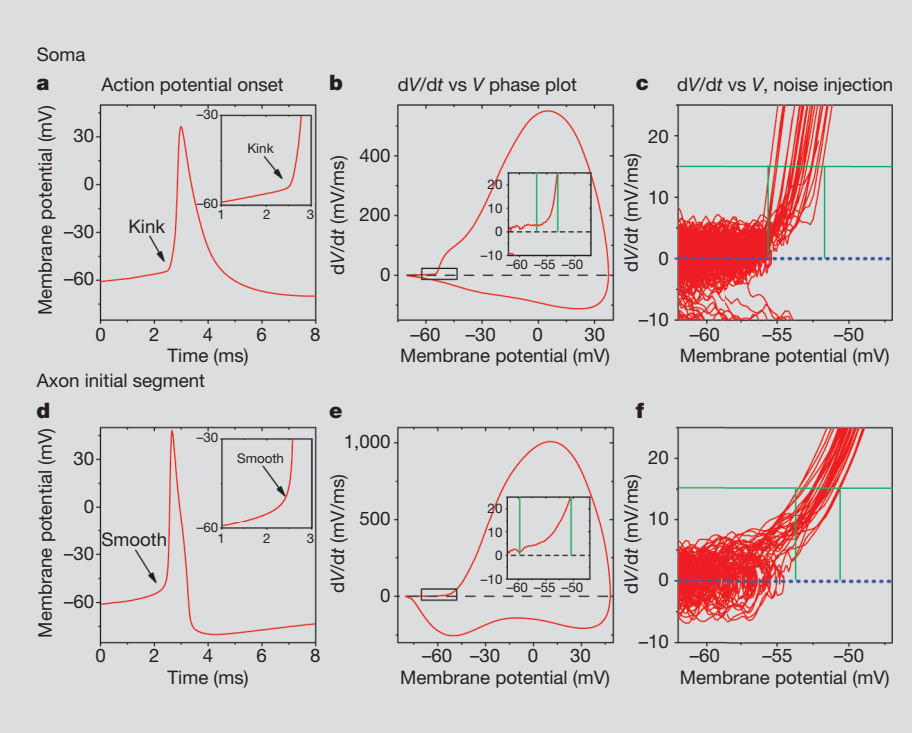

Figure 2 | Hodgkin–Huxley model of a layer-5 cortical pyramidal cell. a, Somatic spike shows a 'kink' at its onset, as in the real neuron. **b,** Phase plot (dV/dt versus V) and close-up of rapid initiation (inset) of the spike shown in **a**. **c,** Close-up of the phase plot of somatic spike during noisy intrasomatic current injection, showing a broad distribution of thresholds (green lines). **d,** Axonal spike (45 μm from the soma). **e,** Phase plot of the axonal spike. Note the smoothly rising dV/dt. **f,** Overlay of dV/dt versus V for the onset of axonal spikes, showing lower variability of spike threshold (green lines).
Methods. Results were obtained from a model layer-5 cortical pyramidal cell[13] with the intrasomatic injection of a 10–15 mV noisy conductance. The model contained the following conductances: soma (Na^+, 0.75 nS μm^{-2}; K^+, 0.15 nS μm^{-2}); axon hillock and initial segment (Na^+, 7.5 nS μm^{-2}; K^+, 1.5 nS μm^{-2}); dendrite (Na^+, 0.1 nS μm^{-2}; K^+, 0.002 nS μm^{-2}; M-current, 0.0003 nS μm^{-2}). Axonal length, 50 μm; soma size, 20 × 30 μm. These parameters were used to match the maximal dV/dt rates, durations and initiation site of spikes in our neurons (Fig. 1). Similar results are obtained from several Hodgkin–Huxley models of cortical pyramidal cells, including those using a high, medium or relatively low density of axonal Na^+ conductance[12–14], and the results from these simulations were well within the range of real cortical cells (see also www.mccormicklab.org).

†Present address: Institute of Neuroscience, Chinese Academy of Science, Shanghai 200031, China

1. Naundorf, B., Wolf, F. & Volgushev, M. *Nature* **440,** 1060–1063 (2006).
2. Palmer, L. M. & Stuart, G. J. *J. Neurosci.* **26,** 1854–1863 (2006).
3. Stuart, G., Schiller, J. & Sakmann, B. *J. Physiol.* **505,** 617–632 (1997).
4. Shu, Y., Duque, A., Yu, Y., Haider, B. & McCormick, D. A. *J. Neurophysiol.* doi:10.1152/jn.00922.2006 (2006).
5. Pare, D., Shink, E., Gaudreau, H., Destexhe, A. & Lang, E. J. *J. Neurophysiol.* **79,** 1450–1460 (1998).
6. Shu, Y., Hasenstaub, A., Duque, A., Yu, Y. & McCormick, D. A. *Nature* **441,** 761–765 (2006).
7. Colbert, C. M. & Johnston, D. *J. Neurosci.* **16,** 6676–6686 (1996).
8. Coombs, J. S., Curtis, D. R. & Eccles, J. C. *J. Physiol.* **139,** 232–249 (1957).
9. Shu, Y., Hasenstaub, A., Badoual, M., Bal, T. & McCormick, D. A. *J. Neurosci.* **23,** 10388–10401 (2003).
10. Inda, M. C., DeFelipe, J. & Munoz, A. *Proc. Natl Acad. Sci. USA* **103,** 2920–2925 (2006).
11. Komada, M. & Soriano, P. *J. Cell Biol.* **156,** 337–348 (2002).
12. Colbert, C. M. & Pan, E. *Nature Neurosci.* **5,** 533–538 (2002).
13. Mainen, Z. F. & Sejnowski, T. J. *Nature* **382,** 363–366 (1996).
14. Baranauskas, G. & Martina, M. *J. Neurosci.* **26,** 671–684 (2006).

doi:10.1038/nature05523

NEUROPHYSIOLOGY

Naundorf et al. *reply*

Replying to: D. A. McCormick, Y. Shu & Y. Yu *Nature* 445, 10.1038/nature05523 (2007)

McCormick *et al.*[1] question whether the rapid onset and highly variable thresholds of action potentials[2] are genuine features of cortical action-potential generators — that is, whether they reflect the voltage-dependence of the underlying sodium currents. Instead, they consider these features to be epiphenomena, reflecting lateral currents from a remote initiation site, and, contrary to direct evidence[3], they assume that sodium currents show canonical kinetics.

Although the lateral current hypothesis of

the AIS (Fig. 2f) than in the soma (Fig. 2c), as we found for real neurons (Fig. 1c, f).

We found that several other Hodgkin–Huxley models of cortical pyramidal cells, even one based on a relatively low density of Na^+ conductance in the axon, replicated the 'kink' and variability of somatic spikes (Fig. 2 legend). These features of spike initiation in the soma were dependent on the initiation of spikes in the AIS: increasing the somatic Na^+ conductance to a high level (7.5 nS μm^{-2}) and removing Na^+ conductance from the axon in the model presented here resulted in a loss of the kink at the foot of the spike (soma slope, 4.1 ms^{-1}) and a reduction in spike threshold variability in the soma (results not shown).

Our findings reveal that leading Hodgkin–Huxley models of cortical pyramidal cell spike initiation capture the so-called unique features observed by Naundorf *et al.*[1]. We attribute these features simply to recording from a site that is distant from the site of spike initiation and to the non-uniform distribution of spike properties over the somatic and axonal membrane. The initiation of spikes in the axon that then back-propagate into the soma can result in a rapid change in membrane potential (the kink) at the foot of the somatic spike. The large current supplied by the axonal spike precedes and overlaps with the current supplied by the local generation of the action potential in the soma during the rising phase of the spike. This results in a more rapid rise at the foot of the spike in the soma than would occur if there were no preceding spike in the axon. The apparent high threshold variability with intrasomatic recordings merely results from membrane potential differences between the soma and the actual site of spike initiation, the axon, at the time that spikes are generated. These membrane-potential differences arise from local electrophysiological differences, as well as spatial non-uniformity in synaptic activity. We conclude that the observations made by Naundorf *et al.*[1] are predictable by Hodgkin–Huxley theory and the known physiology of spike initiation[2–4], and that there is no need to invoke exotic interchannel cooperativity to explain their observations.

David A. McCormick*, Yousheng Shu*†, Yuguo Yu*

*Department of Neurobiology, Kavli Institute for Neuroscience, Yale University School of Medicine, New Haven, Connecticut 06510, USA
e-mail: david.mccormick@yale.edu

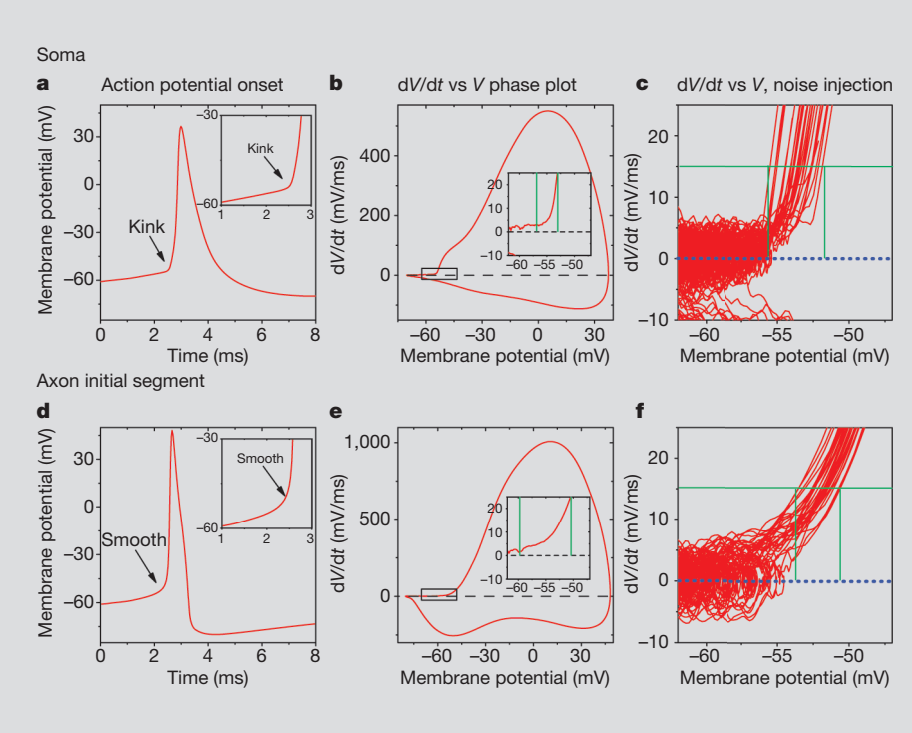

Figure 2 | Hodgkin–Huxley model of a layer-5 cortical pyramidal cell. a, Somatic spike shows a 'kink' at its onset, as in the real neuron. **b,** Phase plot (dV/dt versus V) and close-up of rapid initiation (inset) of the spike shown in **a**. **c,** Close-up of the phase plot of somatic spike during noisy intrasomatic current injection, showing a broad distribution of thresholds (green lines). **d,** Axonal spike (45 μm from the soma). **e,** Phase plot of the axonal spike. Note the smoothly rising dV/dt. **f,** Overlay of dV/dt versus V for the onset of axonal spikes, showing lower variability of spike threshold (green lines).
Methods. Results were obtained from a model layer-5 cortical pyramidal cell[13] with the intrasomatic injection of a 10–15 mV noisy conductance. The model contained the following conductances: soma (Na^+, 0.75 nS μm^{-2}; K^+, 0.15 nS μm^{-2}); axon hillock and initial segment (Na^+, 7.5 nS μm^{-2}; K^+, 1.5 nS μm^{-2}); dendrite (Na^+, 0.1 nS μm^{-2}; K^+, 0.002 nS μm^{-2}; M-current, 0.0003 nS μm^{-2}). Axonal length, 50 μm; soma size, 20 × 30 μm. These parameters were used to match the maximal dV/dt rates, durations and initiation site of spikes in our neurons (Fig. 1). Similar results are obtained from several Hodgkin–Huxley models of cortical pyramidal cells, including those using a high, medium or relatively low density of axonal Na^+ conductance[12–14], and the results from these simulations were well within the range of real cortical cells (see also www.mccormicklab.org).

†Present address: Institute of Neuroscience, Chinese Academy of Science, Shanghai 200031, China

1. Naundorf, B., Wolf, F. & Volgushev, M. *Nature* **440,** 1060–1063 (2006).
2. Palmer, L. M. & Stuart, G. J. *J. Neurosci.* **26,** 1854–1863 (2006).
3. Stuart, G., Schiller, J. & Sakmann, B. *J. Physiol.* **505,** 617–632 (1997).
4. Shu, Y., Duque, A., Yu, Y., Haider, B. & McCormick, D. A. *J. Neurophysiol.* doi:10.1152/jn.00922.2006 (2006).
5. Pare, D., Shink, E., Gaudreau, H., Destexhe, A. & Lang, E. J. *J. Neurophysiol.* **79,** 1450–1460 (1998).
6. Shu, Y., Hasenstaub, A., Duque, A., Yu, Y. & McCormick, D. A. *Nature* **441,** 761–765 (2006).
7. Colbert, C. M. & Johnston, D. *J. Neurosci.* **16,** 6676–6686 (1996).
8. Coombs, J. S., Curtis, D. R. & Eccles, J. C. *J. Physiol.* **139,** 232–249 (1957).
9. Shu, Y., Hasenstaub, A., Badoual, M., Bal, T. & McCormick, D. A. *J. Neurosci.* **23,** 10388–10401 (2003).
10. Inda, M. C., DeFelipe, J. & Munoz, A. *Proc. Natl Acad. Sci. USA* **103,** 2920–2925 (2006).
11. Komada, M. & Soriano, P. *J. Cell Biol.* **156,** 337–348 (2002).
12. Colbert, C. M. & Pan, E. *Nature Neurosci.* **5,** 533–538 (2002).
13. Mainen, Z. F. & Sejnowski, T. J. *Nature* **382,** 363–366 (1996).
14. Baranauskas, G. & Martina, M. *J. Neurosci.* **26,** 671–684 (2006).

doi:10.1038/nature05523

NEUROPHYSIOLOGY

Naundorf et al. *reply*

Replying to: D. A. McCormick, Y. Shu & Y. Yu *Nature* 445, 10.1038/nature05523 (2007)

McCormick *et al.*[1] question whether the rapid onset and highly variable thresholds of action potentials[2] are genuine features of cortical action-potential generators — that is, whether they reflect the voltage-dependence of the underlying sodium currents. Instead, they consider these features to be epiphenomena, reflecting lateral currents from a remote initiation site, and, contrary to direct evidence[3], they assume that sodium currents show canonical kinetics.

Although the lateral current hypothesis of

McCormick *et al.* is superficially plausible, their recordings are inadequate for showing that the dynamics of axonal action-potential initiation conforms to the canonical model. Their so-called axonal recordings are actually obtained from 'blebs' — injury-induced swellings of cut axons on the slice surface. The injured axons, when forming blebs, reorganize their entire cytoskeleton, including the destruction of the sub-membrane spectrin network[4] that integrates sodium channels into the supramolecular machinery of the normal initial segment[5]. As the behaviour of axonal sodium channels is highly sensitive to their cellular environment[6], the smooth action-potential waveforms in the blebs, instead of revealing the true dynamics of action-potential initiation, are more likely to be caused by the disorganized state of the bleb membrane.

The model of McCormick *et al.*[1] does not conform with the known physiology of layer-5 pyramidal cells. Contradicting direct measurements[7,8], it assumes a high ratio of axonal-to-somatic sodium currents. Even with these physiologically unrealistic settings, their model still does not reproduce the experimental data. In their *in vitro* recordings, as in our *in vivo* recordings (Fig. 2 (panels a, c) in ref. 2), somatic action potentials rise almost vertically out of the cloud of subthreshold fluctuations. In their model, however, the range of action-potential onset potentials hardly overlaps with the range of subthreshold fluctuations, being shifted towards more depolarized potentials (Fig. 2 (panel c) in ref. 1). The model of McCormick *et al.* therefore in fact provides further evidence that canonical models are incapable of correctly describing the observed dynamics of action-potential initiation[2,3].

However, McCormick *et al.* highlight an important issue. How can the action-potential dynamics at a remote initiation site be critically probed, when action-potential waveforms recorded from thin processes, such as axons, are likely to be compromised by technical problems[9]? Our analysis identifies an essentially non-invasive approach for addressing this question (see supplementary information of ref. 2). It is based on quantifying the ability of a neuron to phase-lock its spikes to a weak test stimulus in the irregular firing regime[2,10,11].

Theoretical studies indicate that canonical generators of action potentials have a very limited ability to encode high-frequency inputs, showing cut-off frequencies of phase-locking (v_c) that are of the order of their mean firing rate[10,11]. By contrast, models with intrinsically high onset rapidness (r) can show arbitrarily high cut-off frequencies[2,10–12]. If the rapidness of the action-potential onset is genuinely increased by a factor of 10, then cut-off frequencies above 100 Hz are predicted by dimensional analysis ($v_c \propto r$), even for mean firing rates of around 10 Hz. Both *in vivo* and *in vitro* studies have revealed signatures of such fast responses in the neocortex[12,13], supporting genuinely rapid initiation of action potentials in cortical neurons (see also http://www.nld.ds.mpg.de/actionpotentials).

Björn Naundorf*, Fred Wolf*, Maxim Volgushev†
*Max Planck Institute for Dynamics and Self-Organization, Department of Physics and Bernstein Center for Computational Neuroscience, University of Göttingen, 37073 Göttingen, Germany
e-mail: fred@nld.ds.mpg.de
†Department of Neurophysiology, Ruhr-University Bochum, 44780 Bochum, Germany; and Institute of Higher Nervous Activity and Neurophysiology Russian Academy of Science, Moscow 117485, Russia

1. McCormick, D. A., Shu, Y. & Yu, Y. *Nature* **445,** doi:nature05523 (2007).
2. Naundorf, B., Wolf, F. & Volgushev, M. *Nature* **440,** 1060–1063 (2006).
3. Baranauskas, G. & Martina, M. *J. Neurosci.* **26,** 671–684 (2006).
4. Spira, M. E., Oren, R., Dormann, A., Ilouz, N. & Lev, S. *Cell Mol. Neurobiol.* **21,** 591–604 (2002).
5. Lacas-Gervais, S. *et al. J. Cell Biol.* **166,** 983–990 (2004).
6. Rush, A. M., Dib-Hajj, S. D. & Waxman, S. G. *J. Physiol.* **564,** 803–815 (2005).
7. Colbert, C. M. & Pan, E. *Nature Neurosci.* **5,** 533–538 (2002).
8. Ruben, P. C., Ilscher, S. U., Williams, S. R. & Stuart, G. *J. Soc. Neurosci.* abstr. 476.2 (2003).
9. Waters, J., Schaefer, A. & Sakmann, B. *Progr. Biophys. Mol. Biol.* **87,** 145–170 (2005).
10. Fourcaud-Trocme, N., Hansel, D., van Vreeswijk, C. & Brunel, N. *J. Neurosci.* **23,** 11628–11640 (2003).
11. Naundorf, B., Geisel, T. & Wolf, F. *J. Comput. Neurosci.* **18,** 297–309 (2005).
12. Silberberg, G., Bethge, M., Markram, H., Pawelzik, K. & Tsodyks, M. *J. Neurophysiol.* **91,** 704–709 (2004).
13. Williams, P. E., Mechler, F., Gordon, J., Shapley, R. & Hawken, M. J. *J. Neurosci.* **24,** 8278–8288 (2004).

doi: 10.1038/nature05534